

University of Windsor

Scholarship at UWindor

Electronic Theses and Dissertations

Theses, Dissertations, and Major Papers

2005

Optimal control for electrical power-assisted steering system.

Xiaoqun Chen
University of Windsor

Follow this and additional works at: <https://scholar.uwindsor.ca/etd>

Recommended Citation

Chen, Xiaoqun, "Optimal control for electrical power-assisted steering system." (2005). *Electronic Theses and Dissertations*. 2942.

<https://scholar.uwindsor.ca/etd/2942>

This online database contains the full-text of PhD dissertations and Masters' theses of University of Windsor students from 1954 forward. These documents are made available for personal study and research purposes only, in accordance with the Canadian Copyright Act and the Creative Commons license—CC BY-NC-ND (Attribution, Non-Commercial, No Derivative Works). Under this license, works must always be attributed to the copyright holder (original author), cannot be used for any commercial purposes, and may not be altered. Any other use would require the permission of the copyright holder. Students may inquire about withdrawing their dissertation and/or thesis from this database. For additional inquiries, please contact the repository administrator via email (scholarship@uwindsor.ca) or by telephone at 519-253-3000ext. 3208.

Optimal Control for Electrical Power-assisted Steering System

by
Xiaoqun Chen

A Thesis

Submitted to the Faculty of Graduate Studies and Research
through Electrical Engineering
in Partial Fulfillment of the Requirements for the Degree of Master of
Applied Science at the
University of Windsor

Windsor, Ontario, Canada

©XIAOQUN CHEN 2005



Library and
Archives Canada

Bibliothèque et
Archives Canada

Published Heritage
Branch

Direction du
Patrimoine de l'édition

395 Wellington Street
Ottawa ON K1A 0N4
Canada

395, rue Wellington
Ottawa ON K1A 0N4
Canada

Your file *Votre référence*
ISBN: 0-494-09783-3
Our file *Notre référence*
ISBN: 0-494-09783-3

NOTICE:

The author has granted a non-exclusive license allowing Library and Archives Canada to reproduce, publish, archive, preserve, conserve, communicate to the public by telecommunication or on the Internet, loan, distribute and sell theses worldwide, for commercial or non-commercial purposes, in microform, paper, electronic and/or any other formats.

The author retains copyright ownership and moral rights in this thesis. Neither the thesis nor substantial extracts from it may be printed or otherwise reproduced without the author's permission.

AVIS:

L'auteur a accordé une licence non exclusive permettant à la Bibliothèque et Archives Canada de reproduire, publier, archiver, sauvegarder, conserver, transmettre au public par télécommunication ou par l'Internet, prêter, distribuer et vendre des thèses partout dans le monde, à des fins commerciales ou autres, sur support microforme, papier, électronique et/ou autres formats.

L'auteur conserve la propriété du droit d'auteur et des droits moraux qui protègent cette thèse. Ni la thèse ni des extraits substantiels de celle-ci ne doivent être imprimés ou autrement reproduits sans son autorisation.

In compliance with the Canadian Privacy Act some supporting forms may have been removed from this thesis.

Conformément à la loi canadienne sur la protection de la vie privée, quelques formulaires secondaires ont été enlevés de cette thèse.

While these forms may be included in the document page count, their removal does not represent any loss of content from the thesis.

Bien que ces formulaires aient inclus dans la pagination, il n'y aura aucun contenu manquant.


Canada

Abstract

An electric power-assisted steering (EPS) system has been gradually used to replace hydraulic power steering (HPS) in recent years. In an EPS system, an electric motor generates assisting steering torque to make comfortable steering operation for drivers.

To achieve better driving feeling in the EPS system, there are three problems need to be addressed: Sufficient assist torque should be transferred to drivers ; road roughness and road reaction torque shall be taken by the controller; system transient response shall be accelerated by the controller. Various control algorithms have been derived now, however, most of them are derived simply based on the motor model [1],[6] and given this design strategy, they are not able to handle and consider the full system specifications very well.

In this thesis, a new controller structure design is proposed for an EPS system that addresses disturbance attenuation, offering sufficient gain and achieve system transient response at the same time. We introduced a new two control strategy to design the controller that incorporates a motion controller and a motor torque controller in different loops. The motion controller is an optimal H_2 controller which takes care of the disturbance attenuation and accelerate system transient response issues. The motor controller is a $P - I$ controller that is used to generate sufficient assistant torque according to the command input from the motion controller.

The simulation for the whole EPS system is implemented by *CarSim* and simulink. *CarSim* will simulate the road reaction torque and the EPS model is built on the simulink platform. All the results are not only tested under the off-line simulations, but also transformed to a real-time format and verified through real-time simulations. In both cases, it fulfills the control objectives and achieves good performance.

Acknowledgment

I would like to acknowledge my deepest gratitude and indebtedness to Dr. Xiang Chen, my supervisor, for his encouragement, sincere guidance, friendly supervision and valuable suggestion. Without his continuous help, this research would not be possible to be accomplished. I wish to take this opportunity to express my great thankfulness and respect to Dr. Xiang Chen.

This research is supported in part by NSERC, also thanks to the financial support from them.

I also would like to thank to Dr. N. Kar, the internal reader from the Department of Electrical and Computer Engineering, and Dr. Jessica Chen, the external reader from the Department of Computer Science, for their valuable suggestions during the evaluation of this thesis and the seminars.

I am very grateful for Alan Soltis, an application engineer from Opal-RT, he gave me great help on realizing the real-time simulation. And I am also wish to thank engineers from *Carsim* for their kindly onsite technical support.

I am very grateful to the Department of Electrical and Computer Engineering for the support of my graduate studies in these two years. I am also grateful to my fellow graduate students in the department for their continuous support and encouragement during the entire progress of the work.

Contents

Abstract	iii
Acknowledgment	iv
List of Figures	vii
1 Introduction	1
1.1 EPS and HPS Systems	1
1.2 Modeling An EPS System And Modeling Survey	2
1.3 Controller of EPS System	4
1.4 Research Objectives and Thesis Structure	5
2 EPS Dynamic Model	7
2.1 Dynamic Model for EPS System	7
2.1.1 Steering Wheel Dynamics	7
2.1.2 Torque Sensor Dynamics	8
2.1.3 Electric Motor Dynamic with Torque Control	9
2.1.4 Pinion & Rack Dynamic	11
2.2 EPS Model Integration	12
3 H_2 Optimal Control Design Theory	15
3.1 H_2 Norm	15
3.2 H_2 Optimal Control	16

4	Control Design for EPS System	18
4.1	Torque Control Design	19
4.2	H_2 Motion Control Design	21
5	Model Reduction	26
5.1	Model Reduction based on Balance Truncation	26
5.2	EPS Motion Controller Model Reduction	29
6	Simulation	32
6.1	Vehicle Dynamics Setup Using CarSim	32
6.1.1	Steering System Forces and Moments	32
6.1.2	Simulation using CarSim	36
6.2	Test Benchmark Set Up	37
6.3	Off-Line Simulations and Results	41
6.4	Real-Time Simulations	52
7	Conclusion and Future Work	62
7.1	Conclusion	62
7.2	Future work	63
7.2.1	Hardware-in-the-loop	63
7.2.2	Fault Tolerant Implementation	63
	Appendix A - Coefficients used EPS system	64
	Appendix B - CARSIM-RT and OPAL-RT Set up	65
	Bibliography	73
	Vita Auctoris	75

List of Figures

1.1	EPS Schematic Arrangement	2
2.1	EPS Dynamic Model	7
2.2	Steering Wheel Model	8
2.3	Torque Sensor Model	8
2.4	Torque Sensor Model	9
2.5	Brushed DC Motor	10
2.6	Brushed DC Motor Model	10
2.7	Brushed DC Motor Model	11
2.8	Rack & Pinion Model	12
2.9	EPS System Overview	13
3.1	LFT Expression of Control System	16
4.1	Schematic Digram of EPS System	18
4.2	EPS System Overview with New Motion Controller	19
4.3	Motor Control System Block	20
4.4	Motor Response with P-I Controller	20
4.5	System with New Controller Structure	21
4.6	New Simplified Controller Structure	22
4.7	Matlab Augmented System	23
4.8	Weight1 Specification	24
4.9	Weight2 And Weight3 Specification	24

5.1	Comparison between <i>2nd</i> Order Model And Original <i>8th</i> Order Model	31
5.2	Comparison between <i>6th</i> Order Model and Original <i>8th</i> Order Model	31
6.1	Steering Forces and Moments	33
6.2	EPS System Simulation Block Integrated with CarSim	37
6.3	System Input Signal	39
6.4	EPS System Model with a H_2 Motion Controller	40
6.5	Road Reaction Torque and Torque Sensor Output Integrated with H_2 Controller (random number variance = 10)	42
6.6	Human Wheel Position And Rack & Pinion Angle with H_2 Controller (random number variance = 10)	42
6.7	CarSim Output Angle Compared with EPS Output Angle with H_2 Controller (random number variance = 10)	43
6.8	Road Reaction Torque And Torque Sensor Output Integrated with H_2 Controller (random number variance = 50)	44
6.9	Human Wheel Position And Rack & Pinion Angle with H_2 Controller (random number variance = 50)	45
6.10	Road Reaction Torque And Torque Sensor Output without the Motion Controller (random number variance = 50)	46
6.11	Road Reaction Torque And Torque Sensor Output Integrated with $P - I$ Controller, $P=0.05, I=0.3$ (random number variance = 10)	47
6.12	Human Wheel Position And Rack & Pinion Angle with $P-I$ Controller, $P=0.05, I=0.3$ (random number variance = 10)	48
6.13	Human Wheel position And Rack & Pinion Angle with $P-I$ Controller, $P=10, I=5$ (random number variance = 10)	48
6.14	Road Reaction Torque And Torque Sensor Output Integrated with H_2 Controller (<i>6th</i> order controller model, random number var = 10)	49
6.15	Human Wheel Position And Rack & Pinion Angle with H_2 Controller (<i>6th</i> order controller model random number var = 10)	50

6.16	CarSim Output Angle Compared with EPS Output Angle with H_2 Controller (6th order controller model random number var=10)	50
6.17	Road Reaction Torque And Torque Sensor Output Integrated with H_2 Controller (2th order controller model random number var = 100)	51
6.18	Human Wheel position And Rack & Pinion Angle with H_2 Controller (2nd order controller model random number var=100)	51
6.19	Schematic Diagram of Computer Work	55
6.20	Motor with Controller System block	56
6.21	EPS System Approximated Simulink Model for Real Time Simulation	58
6.22	Road Reaction Torque and Torque Sensor Output Integrated with H_2 Controller (Real-Time Simulation, random number variance = 10)	59
6.23	Human Wheel position and rack and pinion angle with H_2 Controller (Real- Time Simulation, random number variance = 10)	59
6.24	Carsim Output Angle And EPS Output Rack& Pinion Angle with H_2 Controller (Real-Time Simulation, random number variance = 10)	60
6.25	CarSim Output Angle And EPS Output Rack& Pinion Angle with H_2 Controller (Real-Time Simulation, random number variance = 10)	61
.1	Open CARSIM-RT	66
.2	CARSIM-RT node configuration	67
.3	OPAL-RT main configuration Window	69
.4	Advanced Settings1	70
.5	Advanced Settings2	71
.6	EPS System Real-Time Model	72

Chapter 1

Introduction

1.1 EPS and HPS Systems

Growing needs for safety and environmental friendliness have led to intensive new steering column-related technologies be developed , in particular, for the EPS systems. The EPS system has some significant advantages over any form of hydraulic power steering (HPS) system, both for the owner of the car and their manufacturers. Compared with the HPS, the EPS promises weight reduction, fuel savings and package flexibility, at no cost penalty.

The fact that the EPS system have a much lower engine load, which can be as low as 4W when the car is being driven straightly, means that the fuel economy of a car equipped with EPS is very similar to that of a car with no form of power steering. In fact, analysis provided by manufacturers of EPS systems indicates potential fuel savings of 4 to 8 percent over cars equipped with conventional HPS, partly because the EPS have a lighter mass. Besides, the independence of the EPS system from engine operation also means that should the engine stall, steering assistance does not vary, while in a conventional HPS system, a stalled engine immediately reduces steering assistance to zero, which can be a huge disadvantage if this occurs part way around a tightening corner. From a manufacturer's perspective, the EPS system has great cost benefits. Using EPS reduces assembly line time, allows easy software tuning of the steering assistance characteristics to suit a variety of cars (eg, a sports car or a limousine) and has the potential to improve reliability, which is supported by the statistics that over 50 percent of all power steering warranty claims are from pump and hose problems.

Switching from HPS to EPS, there is also huge environmental gains from the decreased production and disposal of hydraulic fluid and the decreased requirement for the non-recyclable polymers used in hydraulic hoses.

In a conventional HPS system, the response characteristics mainly depend on the dynamic hydraulic value unit and the characteristics of the flowing amount of fluid. So it is extremely difficult to set a power steering system to give optimum frequency characteristics, because of the mechanical features of the HPS system. EPS systems have the different story. It is easy to set system dynamics and the system is also well analyzed in the frequency domain. So compared with HPS, it is much easier to analyze and design a controller with EPS.

1.2 Modeling An EPS System And Modeling Survey

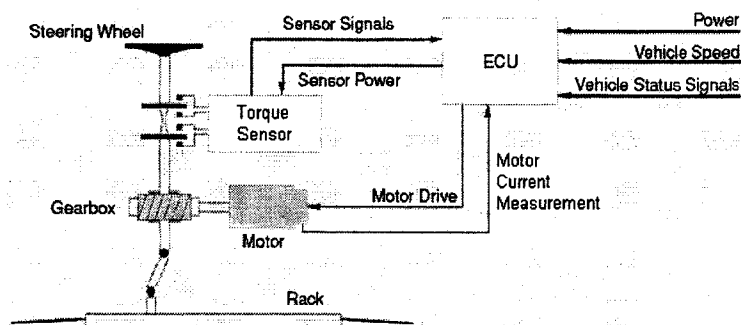


Figure 1.1: EPS Schematic Arrangement

As can be seen from Figure 1.1, an EPS system consists of a torque sensor, an electric control unit (ECU), a reduction gear, a steering wheel, an intermediate shaft (I-Shaft) and a Rack & Pinion. The torque sensor detects driver input and communicates with an electrical control module for processing. The ECU guides motor to accurately deliver the required steering assistance. The torque sensor estimates the torque, which is the command from the human to turn the steering wheel, through the torsion bar mechanism inside. The reduction gear increases the turning force from the motor and transfers it to the steering mechanism. A rack & pinion component is a part of the EPS system to make the tires turn.

The control procedure of the EPS system is summarized as follows:

- 1) The ECU calculates the assistant torque based on the command torque (from torque sensor), the vehicle speed (from speed sensor or in-vehicle network) and the status of the electric motor, and then sends the command to the electric motor.
- 2) The electric motor generates the assistant torque according to the command from the ECU and transfers to the column through a worm gear mechanism.
- 3) The rack and pinion transfers the force through kingpin to tires according to the power assistance from the electric motor.

There are some research activities on powersteering system. A reduced EPS dynamic model was introduced by Delphi to analyze various closed loop effects such as torque performance, disturbance rejection, noise rejection, road feel and stability [2]. This EPS system, named E-SteerTM, consists of a steering column, a gear assist mechanism attached to the column, a brushless DC (BLDC) motor, a controller and a sensor within the assist housing. The main purpose of the steering system was to provide assist torque to the driver. Two main assist algorithms were implemented in the electric control unit. The first was called "Return Algorithm" and the second was called "Damping Algorithm". These two algorithm utilized the position information and provided additional steering functionality. Both algorithms guaranteed the wheel to turn back to the exact center position after the turning.

In [15], a design and implementation method of an EPS system was developed. Four kinds of motors and their respective drivers were proposed, with their advantages and disadvantages compared to one another. An easy solution for trade off among these systems may be achieved when designing the EPS system following the idea in the paper.

A steer-by-wire method was introduced in [6]. It was a big progress for the EPS system, because there was no need for the steering column by using this method. Due to the removal of many mechanical components in the system, more space can be spared inside the vehicle. Moreover, the vehicle cost can be reduced.

1.3 Controller of EPS System

There are several control algorithms which have been conducted in relation to power-steering systems. The system performance, stability and faster response are three key points which need to be considered. Performance is evaluated by how well the system tracks any arbitrary reference trajectory. In our system we also consider whether the system can offer comfortable driving feeling as part of the performance. Stability is an indication of whether the system will reach a stable steady-state value, or in the other way become unstable and crash. The transient response of the system is also an important criteria to evaluate the controller. Practically it can be defined as how fast the tire angle will follow the steering wheel angle change in one cycle.

For system performance, the driver's feeling during steering process is the key[1],[3]. Therefore an important goal to develop a control mechanism for power steering system is to improve the reaction torque vibration on the hand wheel.

In [7], control of a hydraulic power steering system is discussed. In a power steering system, the effectiveness of control has to be evaluated for both system performance and stability.

In [11], the road information was regarded as a frequency band of tire/steering wheel transmission characteristics. A robust controller, which was fulfilled using H_∞ controller, was developed to improve the steering feel as perceived by the driver and guarantee a sufficient assist torque. Several specifications were proposed to guide the design of the controller so that the control device can change the power steering system transmission characteristics without varying the assist force.

In [8], the electric power-assisted steering control is designed for a double pinion type model, where two control strategies are designed for two-input and one output system. Using co-simulation technology, an integrated simulation of an EPS control system with a full vehicle model was developed in [14]. There were two computer nodes that implemented the data communication, concurrently performed to resolve the multi-body dynamics and complex control algorithm and investigated the influence of EPS on the vehicle riding and

handling response. A P-I controller was designed for the whole EPS system and was used to handle the response from the steer and road inputs, which were analyzed and compared as the ground experimental data. A software called "ADAMS" was used to study vehicle dynamics and matlab/simulink was used to implement the sophisticated controller model.

1.4 Research Objectives and Thesis Structure

According to the research of the ECU of the EPS system, there are three key principles as follows:

1. The system requires sufficient assistant torque to the drivers.
2. The system can take care the road roughness and road reaction torque.
3. The faster the transient response system achieves, the better performance system can get.

Different kinds of EPS dynamic models and control strategies have been developed according to practical steering systems. In my research, the controller is to be designed to cover all above three requirements to achieve a good overall system performance. A new optimal H_2 controller based EPS system is developed, in which we adopt a two-degree controller design strategy that has many advantages over traditional controller design methods. Once the controller design is finished, it needs to be considered whether the designed controller can be applied practically in the industries. Normally simple models have advantages over complex models for cost saving and computational efficiency. Therefore we need to develop and apply a model reduction method to the designed controller to decrease its model complexity without losing any significant system performance.

The proposed two-controllers consists of two kinds of controllers: the motion control and the torque control. The distinguished feature of the new controller architecture is that it separates the traditional controller design structure into two separate parts. It enhances the system performance while offering more flexibility to future designs. In the two controller

structure, the motor controller is used to generate the assistant force from the torque sensor output to drive the electric motor. It is required that the controller track the motion control input command as quickly as possible. The motion controller is designed to take care the disturbance from road disturbance in order to provide a comfortable driving feeling. Besides, it is also used to accelerate the overall system transient response.

The remaining of the thesis is organized as follows: in Chapter 2, the whole EPS system model is derived. In Chapter 3, the preliminary optimal control theories, the H_2 theories is introduced, and later will be applied in our presented controller design method. In Chapter 4, the new two controller design method is presented. The model reduction theory and its application to our controller design is presented in Chapter 5. In Chapter 6, the setting up of vehicle dynamics of the tire model , various off-line and real-time simulations are conducted to demonstrate the effectiveness of the designed controller implementing into the system. Chapter 8 concludes the thesis and gives some future perspectives.

Chapter 2

EPS Dynamic Model

2.1 Dynamic Model for EPS System

The EPS system modeling consists of the modeling of the related mechanical components (i.e. the steering wheel, the torque sensor, the electric motor and the pinion & rack), which can be done using the Matlab/simulink tool and has an overall structure as shown in Figure 2.1.

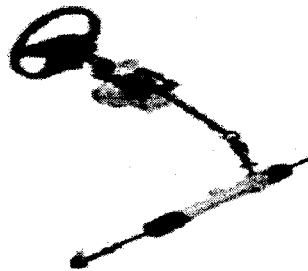


Figure 2.1: EPS Dynamic Model

2.1.1 Steering Wheel Dynamics

The dynamic model of the steering wheel is shown in Figure 2.2.

With the model, a differential equation of the steering wheel can be developed as:

$$T_{hw} - T_s = J_{hw}\ddot{\theta}_{hw} + B_{hw}\dot{\theta}_{hw} + K_{hw}\theta_{hw}, \quad (2.1)$$

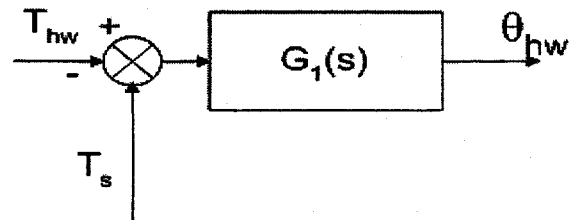


Figure 2.2: Steering Wheel Model

where T_h and T_s are the torques given by the driver and the torque sensor, respectively. θ_{hw} denotes the rotation angle of the steering wheel. J_{hw} , B_{hw} and K_{hw} represent the moment of inertia, the damping coefficient and the stiffness coefficient, respectively. If the steering wheel is rigidly connected, the stiffness coefficient K_{hw} can be neglected, which leads to a simplified model.

Using the Laplace transform, the model's transfer function can be derived in (2.2):

$$\frac{\theta_{hw}}{T_h - T_s} = \frac{1}{J_{hw}S^2 + B_{hw}S} \quad (2.2)$$

2.1.2 Torque Sensor Dynamics

The torque sensor is modeled as a torsion bar and its dynamic model is shown in Figure ??

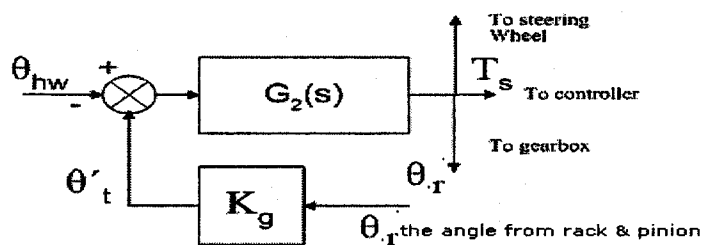


Figure 2.3: Torque Sensor Model

The differential equation of the torque sensor can be derived as:

$$\begin{cases} T_s = K_s(\theta_{hw} - \theta'_t) + B_s \frac{d(\theta_{hw} - \theta'_t)}{dt}, \\ \theta'_t = \theta_r \times K_g, \end{cases} \quad (2.3)$$

where K_s, B_s denote the stiffness coefficient and damping rate of the torsion bar, respectively. θ_v represents the rotation angle of the tire. θ_r represents the rotation angle of the rack & pinion. K_g is the ratio of the steering angle and tire angle. T_s is the torque sensor torque. Using the Laplace transform, a transfer function can be derived in (2.5):

$$\frac{T_s}{\theta_{hw} - \theta_t} = B_s S + K_s; \quad (2.4)$$

In order to simplify the model we do the transformation from Figure?? to Figure ?? Then

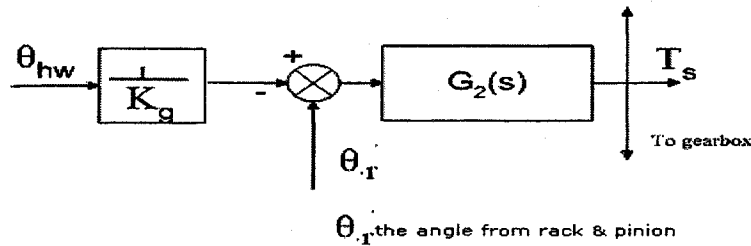


Figure 2.4: Torque Sensor Model

the final torque sensor model equation will be

$$\frac{T_s}{\theta_{hw}/K_g - \theta_r} = B_s S + K_s; \quad (2.5)$$

2.1.3 Electric Motor Dynamic with Torque Control

A common actuator in an EPS system is the DC motor. It directly provides rotary motion and, coupled with wheels or drums and cables, can provide translational motion. The electric circuit of the armature and the free body diagram of the rotor are shown in Figure 2.5.

From Figure 2.6, the motor's equation can be derived based on the Newton's law combined with the Kirchhoff's law, as shown in (2.6).

$$\begin{cases} J_m \ddot{\theta}_m + B_m \dot{\theta}_m = T_m - T_g, \\ L_m \frac{di}{dt} + R_m i = v - K \dot{\theta}_m, \\ T_m - T_g = (J_m S^2 + B_m S) \theta_m, \\ T_m = K i \end{cases} \quad (2.6)$$

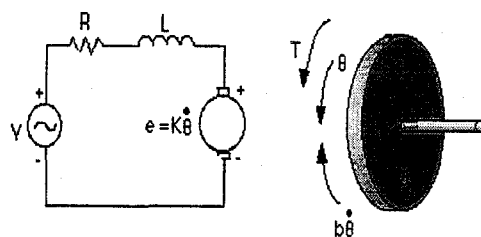


Figure 2.5: Brushed DC Motor

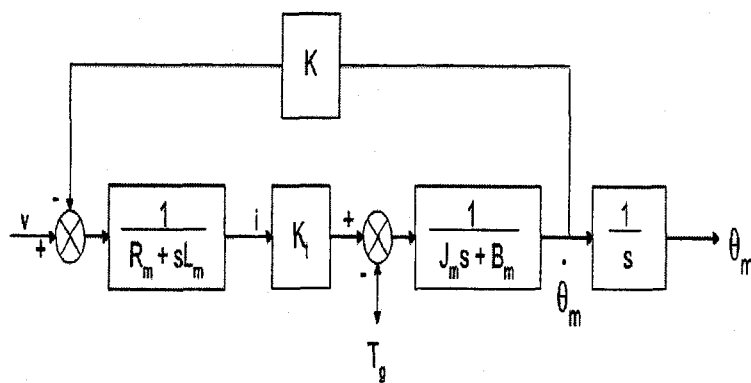


Figure 2.6: Brushed DC Motor Model

Where

Nomenclature

J_m moment of inertia of the rotor
 B_m damping ratio of the mechanical system
 K electromotive force constant
 R_m electric resistance
 L_m electric inductance

T_m Torque generated by motor

T_g Torque generated by the load

If the motor model include the controller, the block diagram structure is shown in Figure 2.7.

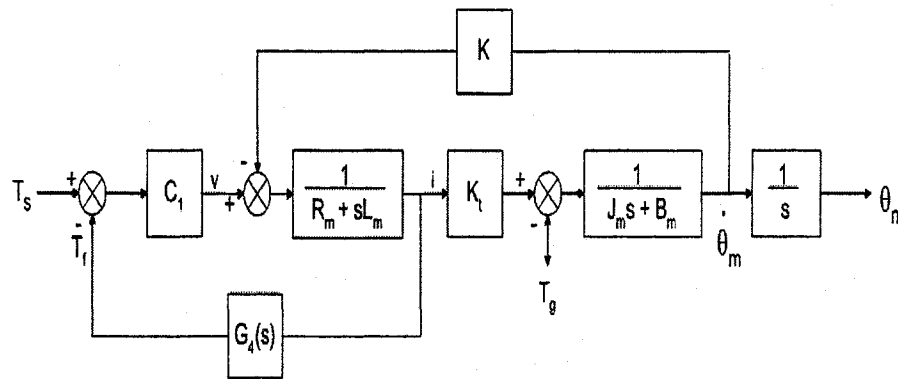


Figure 2.7: Brushed DC Motor Model

2.1.4 Pinion & Rack Dynamic

The pinion & rack is modeled as a mechanic system that consists of a mass and a spring.

The differential equation of the steering wheel is given in (2.7),

$$\begin{cases} T_r + T_s + T_G = J_r \ddot{\theta}_r + B_r \dot{\theta}_r + K_r \theta_r, \\ T_G = n T_g, \\ T_g = T_m - (J_m S^2 + B_m S) \theta_m. \end{cases} \quad (2.7)$$

where J_r , B_r and K_r represent the moment of inertia, the damping coefficient and the stiffness coefficient, respectively. T_r and T_s denote the road wheel torque and the torque sensor torque. T_G denotes the gear torque on the rack and pinion shaft, θ_r represents the rack and pinion angle. The dynamic model of the pinion & rack is shown in Figure 2.8.

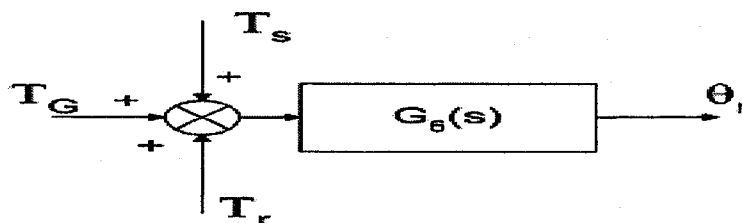


Figure 2.8: Rack & Pinion Model

If the stiffness coefficient K_r is assumed to be zero, the model can be simplified. Using the Laplace transform, a transfer function can be derived in (2.8):

$$\frac{\theta_r}{T_s + T_G + T_r} = \frac{1}{(n^2 J_m + J_r)S^2 + (n^2 B_m + B_r)S}; \quad (2.8)$$

2.2 EPS Model Integration

The EPS system is modeled as a multi-input, multi-output (MIMO) system, as can be seen from the simulink model created according to a real EPS system (Figure 2.1).

The inputs of the EPS system are:

- 1) The command from the driver, which is the torque the driver imposes on the steering wheel, measured in Nm.
- 2) The road information, which is the torque the road wheels feedback to the rack & pinion mechanism, measured in Nm.

The outputs of the EPS system are:

- 1) The steering wheel position, which is the steering angle, measured in degree.
- 2) The road wheel position, which is the angle of the road wheel, measured in degree.
- 3) The road feel to the driver, which is indicated by the torque sensor output, measured in Nm.

The EPS system also has some other mechanical connections, e.g. the deduction gear, which can be assumed as rigid connections. The deduction gear is modeled as a gain with the ratio of 20. The torque from the torsion bar and the torque transmitted through the deduction gear from the assist motor are added up to supply the turning force to the pinion.

An overview of the EPS model in Figure 2.9, based on which the controller will be designed.

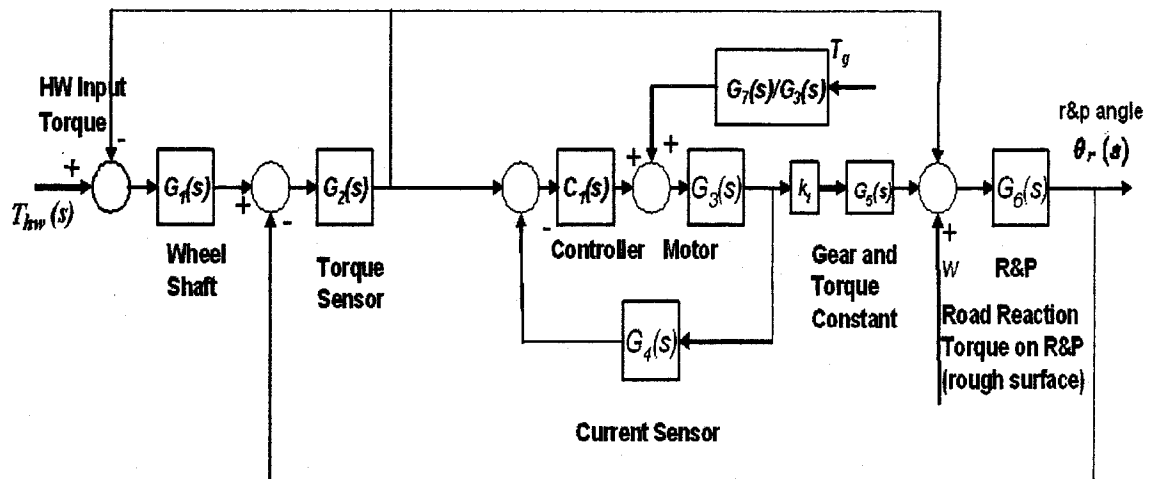


Figure 2.9: EPS System Overview

Nomenclature

G_1 : The dynamic model of the steering wheel.

$$G_1 = \frac{1}{J_{hw}S^2 + B_{hw}S}$$

G_2 : The dynamic model of the torque sensor.

$$G_2 = B_s.S + K_s$$

C : The P-I controller of the motor.

G_3 : The dynamic model of the electric motor.

$$G_3 = \frac{J_m S + B_m}{(J_m S + B_m)(L_m S + R_m)}$$

G_4 : The current sensor.

$$G_4 = K_c$$

G_5 : The dynamic model of the reduction gear.

$$G_5 = K_g$$

G_6 : The dynamic model of the rack and pinion .

$$G_6 = \frac{1}{(n^2 J_m + J_r)S^2 + (n^2 B_m + B_r)S}$$

G_7 : one transfer function in calculation the electro motive force of motor .

$$G_7 = \frac{K}{(J_m S + B_m)(L_m S + R_m)}$$

u : torque from the driver.

w : torque including the noise from the road.

y : angle of the road wheels.

T_g : the load torque used to calculate electro motive force .

Chapter 3

H_2 Optimal Control Design Theory

In this chapter, the theory of the H_2 optimal control is introduced, which will be applied to EPS control design in Chapter 4.

3.1 H_2 Norm

A norm is a real-valued function $\| \cdot \|$ defined on some vector space X (of signals or systems) if it satisfies the following properties:

1. $\| x \| \geq 0$,
2. $\| x \| = 0$ if and only if $x=0$,
3. $\| \alpha x \| = |\alpha| \| x \|$, for any scalar α
4. $\| x + y \| \leq \| x \| + \| y \|$,

for any $x \in X$ and $y \in X$. A real valued function $\| \cdot \|$ is called a semi-norm on X if it satisfies properties 1, 3 and 4 but not necessarily 2.

Given a $G(s) \in RH_\infty$ with a state space realization (A, B, C, D) , we denote

$$G(s) = D + C(sI - A)^{-1}B := \left[\begin{array}{c|c} A & B \\ \hline C & D \end{array} \right],$$

H_2 Control Problem: find a control law $u = K(s)y$ that stabilizes the closed-loop system and minimizes $\|T_{zw}\|_2$, where

$$\|T_{zw}\|_2 = \sqrt{\frac{1}{2\pi} \int_{-\infty}^{\infty} \text{trace}[T_{zw}^*(j\omega)T_{zw}(j\omega)]d\omega}.$$

3.2 H_2 Optimal Control

A basic configuration of the feedback systems considered is shown in Figure 3.1

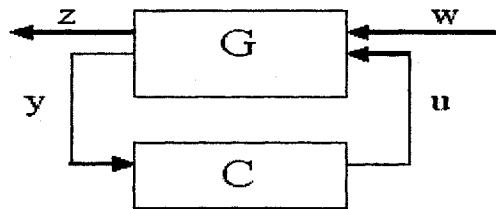


Figure 3.1: LFT Expression of Control System

Nomenclature

- w : The external disturbance or any input signals.
- y : The measurement available to the controller.
- u : The output from the controller.
- z : The error signal that is desired to be kept small.
- C : The controller to be designed.
- G : The conventional plant to be controlled and any weighting functions included to specify the desired performance.

The realization of the transfer matrix G has to take the form

$$G(s) = \left[\begin{array}{c|cc} A & B_1 & B_2 \\ \hline C_1 & 0 & D_{12} \\ C_2 & D_{21} & 0 \end{array} \right]. \quad (3.1)$$

The H_2 problem is to find a proper real-rational controller K that stabilizes G internally and minimizes the H_2 norm of the transfer matrix T_{zw} from w to z , as shown in (3.2).

$$\begin{aligned}\min \|T_{zw}\|_2 &= \lim_{T \rightarrow \infty} \frac{1}{T} E \left\{ \int_0^T z^T z dt \right\} \\ &= \lim_{T \rightarrow \infty} \left\{ \int_0^T (x^T C_1^T C_1 x + u^T D_{12}^T D_{12} + 2x^T C_1^T D_{12} u) dt \right\}.\end{aligned}\quad (3.2)$$

Theorem 3.2.1 [17] : Given the transfer matrix in (3.1), assume:

A1): (A, B_2) is controllable, (C_2, A) is detectable;

A2): D_{12} has full column rank with $[D_{12} D_{\perp}]$ unitary, and D_{21} has full row rank with $\begin{bmatrix} D_{21} \\ D_{\perp} \end{bmatrix}$ unitary, for some D_{\perp} ;

A3): $\begin{bmatrix} A - j\omega & B_2 \\ C_1 & D_{12} \end{bmatrix}$ has full column rank for all ω ;

A4): $\begin{bmatrix} A - j\omega & B_1 \\ C_2 & D_{21} \end{bmatrix}$ has full row rank for all ω .

Then the H_2 control can be achieved by solving two Riccati equations:

$$(A - B_2 R^{-1} D_{12}^T C_1)^T P + P(A - B_2 D_{12}^T C_1) - P B_2 R^{-1} B_2^T P + C_1^T (I - D_{12} R^{-1} D_{12}^T) C_1 = 0, \quad (3.3)$$

$$(A - B_1 D_{21}^T R_2^{-1} C_2)^T Y + Y(A - B_1 D_{21}^T R_2^{-1} C_2) - Y C_2^{-1} R_2^{-1} C_2 Y + B_1 (I - D_{21}^T R_2^{-1} D_{21}) B_1^T = 0, \quad (3.4)$$

where $R = D_{12}^T D_{12} > 0$ and $R_2 = D_{21} D_{21}^T > 0$. From (3.3) and (3.4), Y and P can be obtained and further used to calculate K_f and K_c that involve in the Kalman filter and full-state feedback design, as shown in (3.5) and (3.6).

1) Kalman Filter

$$\begin{cases} \dot{x} = A\hat{x} + B_2 u + K_f (y - C_2 \hat{x}), \\ K_f = -(B_1 D_{21}^T + Y C_2^T) R_2^{-1}. \end{cases} \quad (3.5)$$

2) Full-State Feedback

$$\begin{cases} u = K_c \hat{x}, \\ K_c = -R^{-1} (D_{12}^T C_1 + B_2^T P). \end{cases} \quad (3.6)$$

Note that A1) - A4) are standardized assumptions [17] and the H_2 optimal controller $C(s)$ is realizable in the usual LQG manner as a full-state feedback K_c and a Kalman filter with residual gain matrix K_f .

Chapter 4

Control Design for EPS System

According to the literature survey [1],[6], the most popular EPS controllers are developed based on one single motor control with some compensators as shown in Figure 4.1

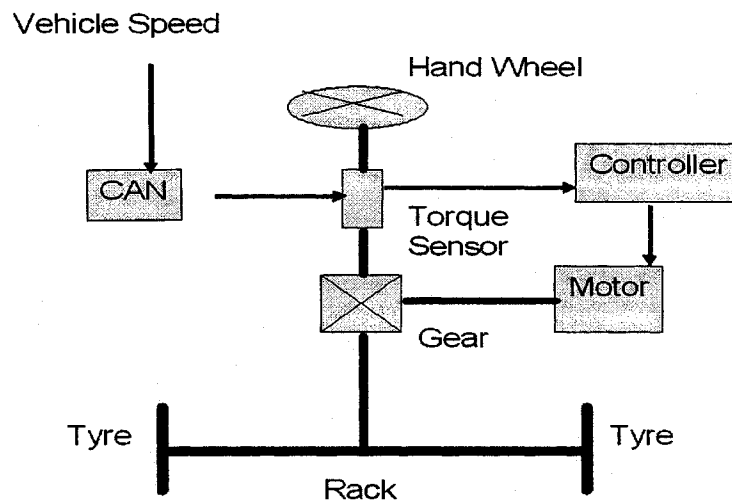


Figure 4.1: Schematic Diagram of EPS System

However, these kinds of controllers not only have their own limitations for considering the overall specifications, but also they had no freedom to extend.

In this chapter, a new controller architecture is proposed in which the EPS control design is inducted in two separate procedures: the motor torque control design and EPS motion control design. The whole EPS system with motion controller block is shown in Figure 4.2.

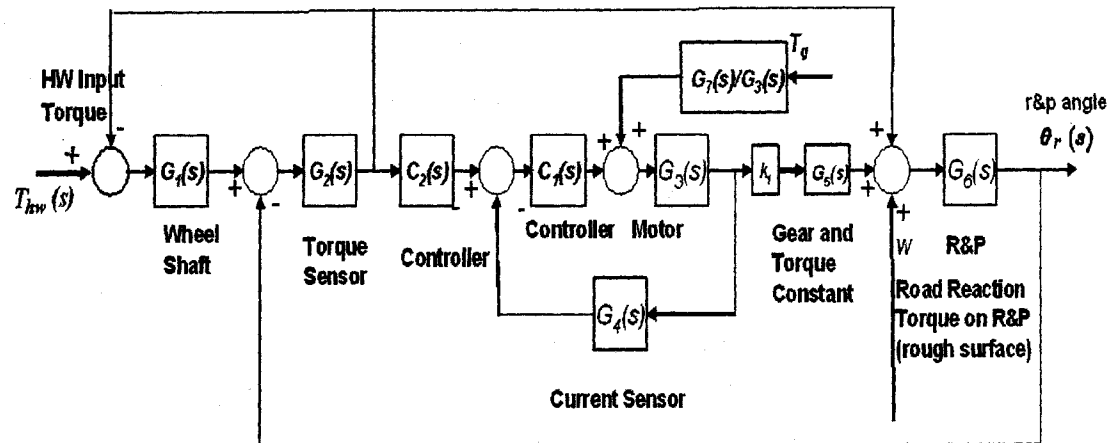


Figure 4.2: EPS System Overview with New Motion Controller

In principle, the torque control is designed to achieve fast motor reaction response to the EPS motion controller input command, and, at the same time to take care of the motor counter balance emf. The EPS motion control is designed in H_2 optimization approach to take care of the EPS transient performance based on the EPS model presented in Chapter 2. The new two controller structure breaks through the limitation of the conventional control structure and leaves space for future more complicated control design such as fault tolerant control. It is noted that both of these controllers can be implemented in the same control unit, so no extra hardware is costed.

4.1 Torque Control Design

In order to design a motor controller, we extract the motor control feedback loop as in Figure 4.3.

The control purpose is to get the fast response of assistant torque, and also take care of the disturbance from the rack and pinion. So in this part, a simple P-I controller is wise choice to implement this function and also to take care of the counter balance EMF. The

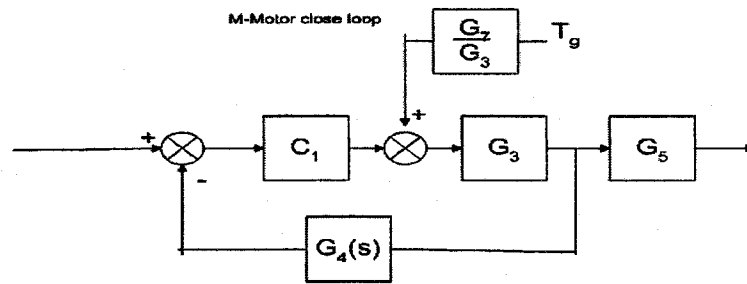


Figure 4.3: Motor Control System Block

motor model transfer function of $\frac{V}{T}$ is indicated by G_3 [10]. Because

$$G_3 = \frac{J_m S + B_m}{(J_m S + B_m)(L_m S + R_m)} \quad (4.1)$$

A P-I controller is derived by error and trial for the motor model as:

$$C_1 = K_p + \frac{K_I}{S} \quad (4.2)$$

$$K_p = 20400, K_I = 700, G_5 = \frac{1}{40} \quad (4.3)$$

G_5 is current sensor

The system response of the motor with the P-I controller is shown in Figure 4.4

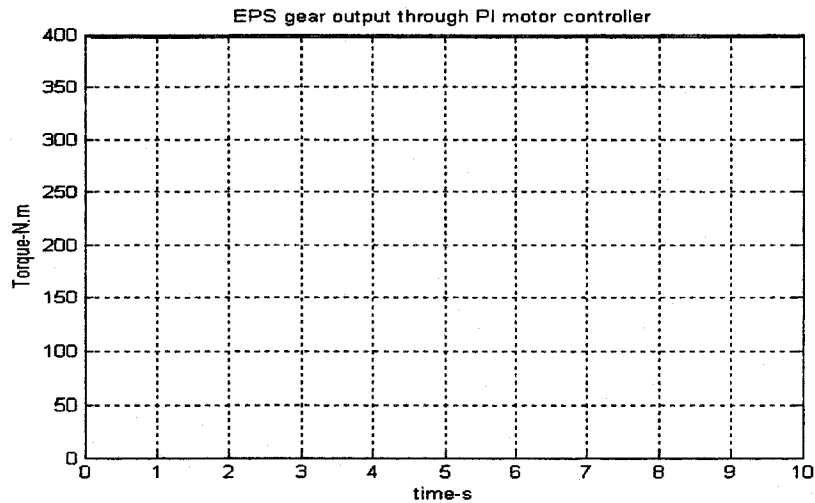


Figure 4.4: Motor Response with P-I Controller

From the Figure 4.4, the P-I control not only takes care of the counter balance EMF, but also makes the motor arrive the stable status in 0.1 seconds.

4.2 H_2 Motion Control Design

In optimal H_2 controller design process, we transform the system block in Figure 4.2 to another form is shown in Figure 4.5 as shown follows:

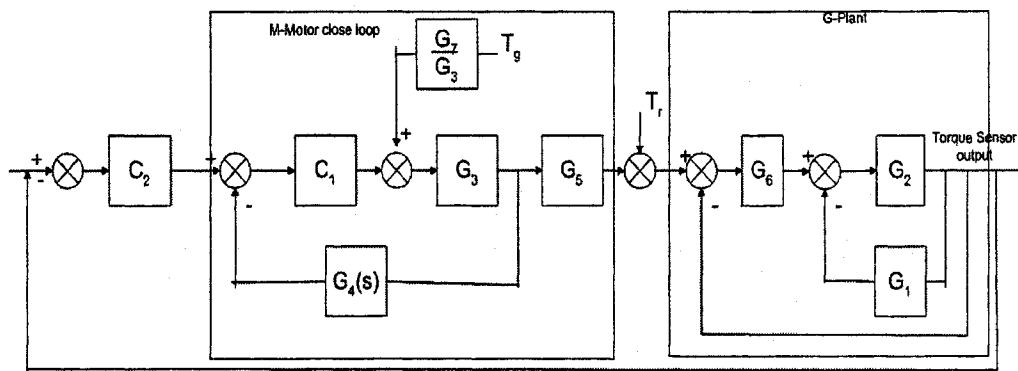


Figure 4.5: System with New Controller Structure

From the system block shown in Fig4.2, there are several problems existed in the system which prevent us designing a controller C_1 to consider both motor control part and motion control for the whole system.

The road disturbance signal, w , is added in the outer feedback loop, but the controller C_1 is in the small motor feedback loop. When the noise come into the system, it is incorporated by other signals. As a result, the controller can not be sensitive to this disturbance signal efficiently.

If there are some model uncertainty exists in the system, the controller as a motor compensator has no freedom to extend to fix this problem.

Based on these problems, we here propose a new way to design the controller for the EPS system. We separate the control unit into two cascade, which can deal with the different plants more efficiently than the conventional controller. From Fig4.5, the master controller C_2 handles the mechanical components of the EPS system so that the system can achieve

better transient response .The slave controller C_1 is specific for the motor response and counter balance EMF control.

Because of the P-I control existing, so counter balance EMF can be omitted when the motion control is designed. From motion controller command input to deduction gear output is the motor with controller close loop transfer function we need. In order to simplify the original system block as shown in Fig4.5 to a classical control system block as shown in Figure 4.6.This transformation will make our design clearer and easier.

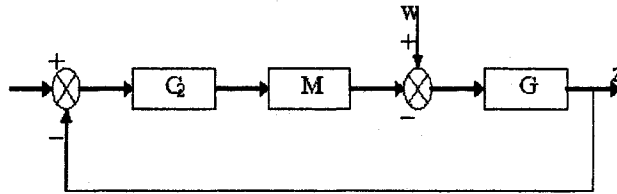


Figure 4.6: New Simplified Controller Structure

C_2 motion controller

M electrical motor+ P-I controller close loop function

Z Torque sensor output

W_1 Road reaction torque , road disturbance

G motion plant

From Figure 4.6, we can see we do the system conversion again. We suppose the whole plant G as the mechanical components of our whole system plant need to be controlled. We derive G as :

$$G = \frac{G_2 G_6}{1 + G_1 G_2 + G_2 G_6}$$

In order to design a controller, we first must check if the plant G in Figure ?? satisfy the assumptions . The state space model for G is as follows:

$$A = \begin{bmatrix} -9.7335 & -207.51 & -1394 \\ 1 & 0 & 0 \\ 0 & 1 & 0 \end{bmatrix}, B = \begin{bmatrix} 1 \\ 0 \\ 0 \end{bmatrix}, \quad (4.4)$$

$$C = [0.03104 \quad 49.684 \quad 30.1] \quad (4.5)$$

$$D = [0] \quad (4.6)$$

An optimal H_2 controller is designed by using Matlab/robust control/toolbox[5]. The optimal H_2 controller try to minimize the cost function as follows.

$$\min \|T_{zw}\|_2 = \lim_{T \rightarrow \infty} \frac{1}{T} E \left\{ \int_0^T z^T z dt \right\} = \lim_{T \rightarrow \infty} \left\{ \int_0^T (x^T C_1^T C_1 x + u^T D_{12}^T D_{12} + 2x^T C_1^T D_{12} u) dt \right\} \quad (4.7)$$

Here $Z = \begin{bmatrix} z_1 \\ z_2 \\ z_3 \end{bmatrix}$ When we design a H_2 controller, we suppose that there exist a torque sensor noise in the system, and also assume that the motion control can take care of this disturbance. When we get the final H_2 controller - C_2 , we still need to check whether the designed H_2 controller can actually work fine with the disturbance signal w or not. According to this design idea, we configure the system as in Figure 4.7. Three weights are also augmented in the system plant to synthesize the final H_2 optimal controller .

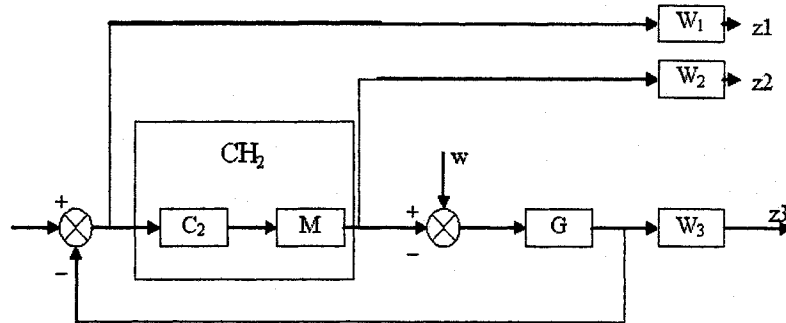


Figure 4.7: Matlab Augmented System

w the disturbance signal from road wheel torque

C_2 the H_2 controller to be designed

M the motor module with a P-I controller

G plant

W_1 weight function penalize the system performance

W_2 a small number to ensure a full rank D_{12} as required by MatLab [5]

W_3 weight function penalize the system robustness.

Considering the weight specification, W_1 as low pass filter can be used to penalize the

system performance.

$$w_1 = 35 \times \frac{(10^6)}{(S^3 + 200S^2 + 2 \times 10^4 S + 10^6)}; w_2 = 0.01; \quad (4.8)$$

W_2 is set to make D_{12} full rank, in order to satisfy the Matlab realization.

$$w_3 = \frac{100}{S}; \quad (4.9)$$

W_3 is used to pass the high frequency noise and error signal so that penalize the system robustness.

The bode plot of the three weights are as follows:

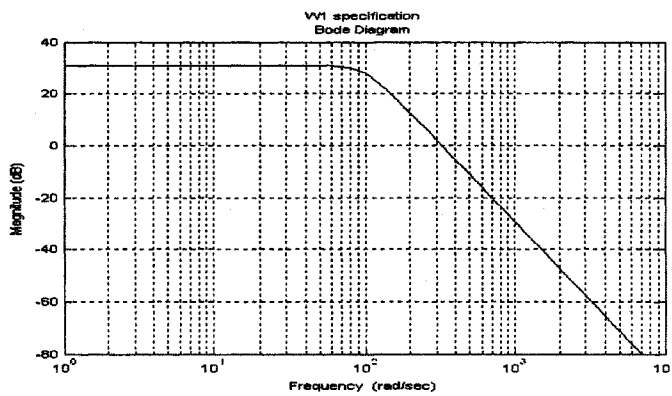


Figure 4.8: Weight1 Specification

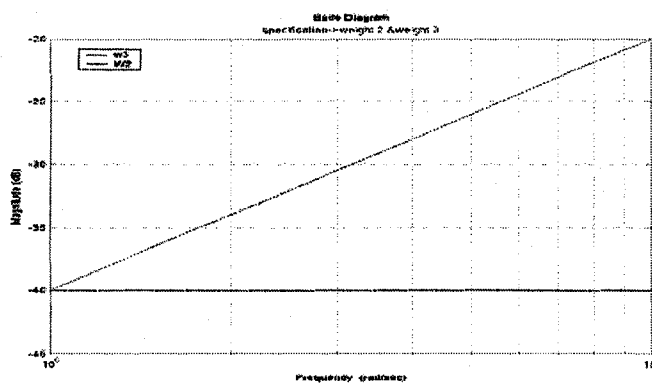


Figure 4.9: Weight2 And Weight3 Specification

Chapter 5

Model Reduction

In this thesis, a new optimal EPS system controller is developed in Chapter 4. The EPS motion controller is an eighth-order controller. However, in terms of the computational efficiency and cost, simple lower-order models are normally preferred. Therefore the application of the techniques that reduce model complexity without losing any significant system performance becomes highly required in some real implementations of the EPS controller systems. In this chapter balanced truncation method is applied to EPS motion controller model reduction. It is shown the objective of reducing computing workload can be effectively achieved.

5.1 Model Reduction based on Balance Truncation

The model order reduction problem can, in general, be stated as: given a full order model $G(s)$, find a lower-order model (say, a r -th order model G_r), such that G and G_r are close in some sense. For example, one may desire that the reduced model be such that $G = G_r + \Delta_a$, with Δ_a very small in H_∞ norm [18]. The model reduction problem can therefore be formulated as:

$$\inf_{\deg(G_r) \leq r} \|G - G_r\|_\infty \quad (5.1)$$

Theorem 5.1.1 [18] : Let $\left[\begin{array}{c|c} A & B \\ \hline C & D \end{array} \right]$ be a state-space realization of a (not necessarily

stable) transfer matrix $G(s)$. Suppose that there exists a symmetric matrix

$$P = P^* = \left[\begin{array}{c|c} P_1 & 0 \\ \hline 0 & 0 \end{array} \right],$$

with P_1 nonsingular such that

$$AP + PA^* + BB^* = 0.$$

Now partition the realization (A, B, C, D) compatibly with P as

$$\left[\begin{array}{cc|c} A_{11} & A_{12} & B_1 \\ A_{21} & A_{22} & B_2 \\ \hline C_1 & C_2 & D \end{array} \right],$$

Then $\left[\begin{array}{c|c} A_{11} & B_1 \\ \hline C_1 & D \end{array} \right]$ is also a realization of G . Moreover, (A_{11}, B_1) is controllable if A_{11} is stable.

Theorem 5.1.2 [18] : Let $\left[\begin{array}{c|c} A & B \\ \hline C & D \end{array} \right]$ be a state-space realization of a (not necessarily stable) transfer matrix $G(s)$. Suppose that there exists a symmetric matrix

$$Q = Q^* = \left[\begin{array}{c|c} Q_1 & 0 \\ \hline 0 & 0 \end{array} \right],$$

with P_1 nonsingular such that

$$QA + A^*Q + C^*C = 0.$$

Now partition the realization (A, B, C, D) compatibly with Q as

$$\left[\begin{array}{cc|c} A_{11} & A_{12} & B_1 \\ A_{21} & A_{22} & B_2 \\ \hline C_1 & C_2 & D \end{array} \right],$$

Then $\left[\begin{array}{c|c} A_{11} & B_1 \\ \hline C_1 & D \end{array} \right]$ is also a realization of G . Moreover, (C_1, A_{11}) is controllable if A_{11} is

stable.

The procedure two theorems suggest that to obtain a minimal realization from a stable nominal realization, one only need to eliminate all states corresponding to the zero block diagonal term of the controllability Gramian P and the observability Gramian Q .

In the special case where Let $\left[\begin{array}{c|c} A & B \\ \hline C & D \end{array} \right]$ is a minimal realization, a balanced realization can be obtained through the following simplified procedure:

1. Compute the controllability and observability Gramians $P > 0, Q > 0$.
- 2) Find a matrix R such that $P=R^*R$.
- 3) Diagonalize RQR^* to get $RQR^* = U\Sigma^2U^2$.
- 4) Let $T^{-1} = R^*U\Sigma^{-1/2}$. Then $TQT^* = (T^*)^{-1}QT^{-1} = \Sigma$ and $\left[\begin{array}{c|c} TAT^{-1} & TB \\ \hline CT^{-1} & D \end{array} \right]$ is balanced.

Theorem 5.1.3 [18] : Consider a stable transfer function G that belongs to RH_∞ , then is balanced realization with Gramian $\Sigma = \text{diag}(\Sigma_1, \Sigma_2)$ (its controllability and observability Gramians are equal and diagonal)

$$G(s) = \left[\begin{array}{cc|c} A_{11} & A_{12} & B_1 \\ A_{21} & A_{22} & B_2 \\ \hline C_1 & C_2 & D \end{array} \right], \quad (5.2)$$

and,

$$\begin{cases} \Sigma_1 = \text{diag}(\sigma_1 I_{s_1}, \sigma_2 I_{s_2}, \dots, \sigma_r I_{s_r}), \\ \Sigma_2 = \text{diag}(\sigma_{r+1} I_{s_{r+1}}, \sigma_{r+2} I_{s_{r+2}}, \dots, \sigma_N I_{s_N}). \end{cases} \quad (5.3)$$

and

$$\Sigma_1 > \Sigma_2 > \dots > \Sigma_r > \Sigma_{r+1} > \Sigma_{r+2} > \dots > \Sigma_N$$

$\sigma_N \ll \sigma_1$ and σ_i has multiplicity $s_i, i = 1, 2, \dots, N$ and $s_1 + s_2 + \dots + s_N = n$.

Then the truncated system

$$G_r(s) = \left[\begin{array}{c|c} A_{11} & B_1 \\ \hline C_1 & D \end{array} \right] \quad (5.4)$$

$$A = \begin{bmatrix} -25.392 & 397.54 & 221.69 & 41.491 & -3.4156 & -60.855 \\ -173.86 & -266.38 & -450.49 & -46.457 & 33.76 & 138.37 \\ -15.673 & -56.227 & -162.38 & -79.495 & -6.4406 & 46.273 \\ -33.24 & 102.35 & 126.27 & -33.842 & -19.281 & -30.056 \\ -10.184 & 33.245 & 40.786 & -16.264 & -9.4953 & -16.1 \\ -16.718 & 62.428 & 67.804 & -44.596 & -28.631 & -80.662 \end{bmatrix}, \quad (5.10)$$

$$B = \begin{bmatrix} -6.0534 \\ 17.642 \\ 10.453 \\ -3.0315 \\ -1.2611 \\ -2.3315 \end{bmatrix}, \quad (5.11)$$

$$C = [4.7023 \quad 15.496 \quad 7.457 \quad -0.93664 \quad -1.3615 \quad -3.1268], \quad (5.12)$$

$$D = [0.00098443]. \quad (5.13)$$

The state space model for the 2nd order after model reduction is shown below:

$$A = \begin{bmatrix} -25.392 & 397.54 \\ -173.86 & -266.38 \end{bmatrix}, \quad B = \begin{bmatrix} -6.0534 \\ 17.642 \end{bmatrix}, \quad (5.14)$$

$$C = [4.7023 \quad 15.496], \quad D = [0.00098443]. \quad (5.15)$$

Comparison between the reduced model and the original model is made in order to check the impact the model reduction brings to the system performance, as can be seen in Figure 5.1 and Figure 5.2.

From the bode plots shown in both figures, we can find the 6th order model is very close to the original model in terms of both magnitude and phase changes. The 2nd order model also tracks the original model quite well. Therefore, through the balance truncation, both reduced order models satisfy the performance requirement. Further details of the reduced models will be discussed in the simulations chapter.

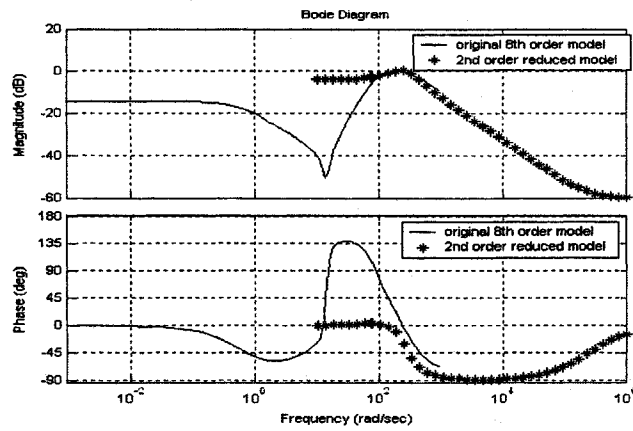


Figure 5.1: Comparison between 2nd Order Model And Original 8th Order Model

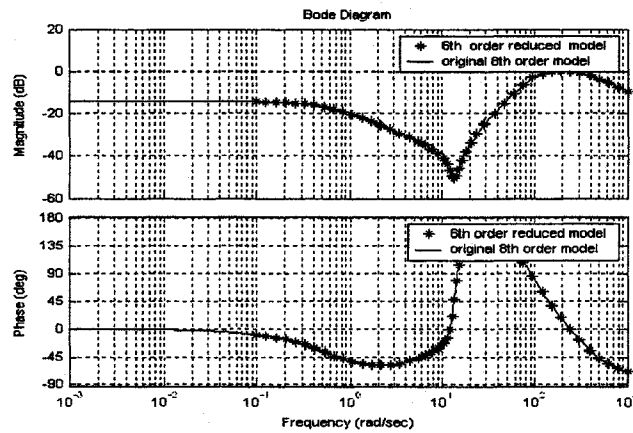


Figure 5.2: Comparison between 6th Order Model and Original 8th Order Model

Chapter 6

Simulation

6.1 Vehicle Dynamics Setup Using CarSim

The function of the steering system is to steer the front wheels in response to the driver command inputs in order to provide an overall directional control of the vehicle. The vehicle dynamic model created considers the front wheel drive mode. The forces and moments that emanate from those generated at the tire-road interface and impose on the steering system are the feedback signals such as the road reaction torque that needs to be simulated and integrated into the EPS model.

6.1.1 Steering System Forces and Moments

The ground reactions on the tire are described by three forces and moments [9], as shown below:

Vertical Force	Aligning torque
Tractive Force	Rolling resistance moment
Lateral Force	Overturning moment

Figure 6.1 shows the three forces and moments acting on a left-hand road wheel. They will be introduced separately to demonstrate their effects on the steering system.

The reaction in the steering system is described by the moment produced on the steer axis, which must be resisted to control the wheel steer angle. Ultimately, the sum of moments from the left and right wheels acting through the steering linkages with their associated ratios

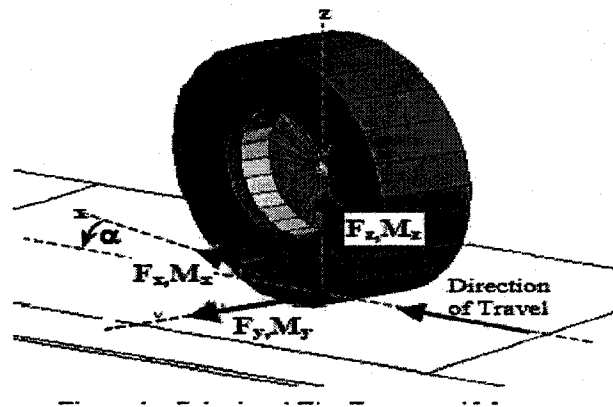


Figure 6.1: Steering Forces and Moments

and efficiencies account for the steering-wheel torque feedback to the driver.

Vertical Force

The vertical load, F_z , acts vertically upward on the wheel and by SAE convention is considered a positive force. Because the steering axis is inclined, F_z has a component acting to produce a moment attempting to steer the wheel. The moments arise from both the caster and lateral inclination angles. Assuming small angles and neglecting camber of the wheel as it steers, the total moment from the two can be approximated by

$$M_V = -(F_{zl} + F_{zr})d \sin \lambda \sin \delta + (F_{zl} - F_{zr})d \sin \nu \cos \delta, \quad (6.1)$$

where:

- F_{zl}, F_{zr} : Vertical load on left and right wheels
- M_V : Total moment from left and right wheels
- d : Lateral offset at the ground
- λ : Lateral inclination angle
- δ : Steer angle
- ν : Caster angle

The first expression on the right side of the above equation arises from the lateral inclination angle, and the last from the caster angle. The sources of each of these moments is most easily visualized by considering the effects of the lateral inclination angle and the

caster angle separately.

The vertical force acting on lateral inclination angle, results in a sine angle force component, $F_{zr} \sin(\lambda)$, which nominally acts laterally on the moment arm " $d \sin(\delta)$ " when the wheel is steered. The moment is zero at zero steer angle. With a steer angle, the moments on both the left and right wheels act together producing a centering moment. The net moment is proportional to the load but independent of left and right imbalance. When steering, both sides of the vehicle lift, and affect which is often described as the source of the centering moment.

The caster angle results in a sine angle force component, $F_{zr} \sin(\nu)$, which nominally acts forward on the moment arm $d \cos(\delta)$. The moments on the left and right wheel are opposite in direction, and tend to balance through the relay linkages. With steer angle, one side of the axle lifts and the other drops, so that the net moment produced depends also on the roll stiffness of the front suspension as it influences the left and right wheel loads.

Lateral Force

The lateral force, F_y , acting at the tire center produces a moment through the longitudinal offset resulting from caster angle. The net moment produced is

$$M_L = -(F_{yl} + F_{yr})r \tan \nu, \quad (6.2)$$

where:

F_{yl}, F_{yr} : Lateral forces at left and right wheels (positive to the right)
 r : Tire radius

The lateral force is generally dependent on the steer angle and conering condition, and with positive caster produces a moment attempting to steer the vehicle out of the turn. Hence, it is a major contributor to understeer.

Tractive Force

The tractive force, F_x , acts on the kingpin offset to produce a moment, which is

$$M_L = -(F_{xl} + F_{xr})d, \quad (6.3)$$

where:

F_{xl}, F_{xr} : Tractive forces at left and right wheels(positive forward)
 r : Tire radius

The left and right moments are opposite in direction and tend to balance through the relay linkage. Imbalances, such as may occur with a tire blowout, brake malfunction, or split coefficient surfaces, will tend to produce a steering moment which is dependent on the lateral offset dimension.

Aligning Torque

The aligning torque, M_z , acts vertically and may be resolved into a component acting parallel to the steering axis. Since moments may be translated without a change in magnitude, the equation for the net moment is:

$$M_{AT} = -(M_{zl} + M_{zr})\cos\sqrt{\lambda^2 + \nu^2}, \quad (6.4)$$

where:

M_{zl}, M_{zr} : Aligning torques on the left and right wheels.

Under normal driving conditions, the aligning torques always act to resist any turning motion, thus their effect is understeer. Only under high braking conditions do they act in a contrary fashion.

Rolling Resistance and Overturning Moments

These moments at most only have a sine angle component acting about the steer axis. They are second-order effects and are usually neglected in analysis of steering system torques.

Equations (6.1) through (6.4) describe the moments input to the steer axis of each road

wheel that comes from the forces and moments acting on the tires. The reactions can be summed up directly to determine the torque feedback to the steering wheel if needed.

6.1.2 Simulation using CarSim

CarSim includes math models that can be loaded and run by Simulink - a software package for modeling, simulating and analyzing dynamical systems. In general, simulink runs under MATLAB, a mathematical workshop.

The input and output signals of the EPS simulink model are as follows: As for the CarSim system, the steering wheel position will be the input signal. As for the output, the steering wheel torque after times the gear defined in the Carsim model, which is calculated using the total moment of the left and the right kingpins of the front wheels, will be an output of the CarSim system and be an input signal as road disturbance to the EPS model at the same time. All the inputs and outputs of the CarSim system is defined as follows:

INPUTS:

- 1) IMP-STEER-SW, which is the steering angle generated by the driver.

OUTPUTS:

- 1) Steer-L1, which is the front left tire angle.
- 2) Steer-R1, which is the front right tire angle.
- 3) V_x , which is the vehicle speed.
- 6) M-SW, which is the steering wheel torque to the EPS system.

In this chapter, offline and real time simulations are designed and conducted to demonstrate the effectiveness of the proposed controller design method, which includes two-degree design strategy, model design and model reduction. First, experiments are conducted on the

G_3 : The dynamic model of the electric motor.

$$G_3 = \frac{J_m S + B_m}{(J_m S + B_m)(L_m S + R_m)}.$$

G_4 : The current sensor.

$$G_4 = K_c.$$

G_5 : The dynamic model of the reduction gear.

$$G_5 = K_g.$$

G_6 : The dynamic model of the rack and pinion .

$$G_6 = \frac{1}{(n^2 J_m + J_r) S^2 + (n^2 B_m + B_r) S}.$$

G_7 : one transfer function in calculation the disturbance to motor .

$$G_7 = \frac{K}{(J_m S + B_m)(L_m S + R_m)}.$$

G_8 : one transfer function in calculation the disturbance to motor .

$$G_8 = n J_m S^2 + n B_m S.$$

u : The torque from the driver.

w : The torque including the white noise from the road.

y : The angle of the road wheels.

The road reaction torque as vehicle dynamics is hard to be modeled. Using the commercial software CarSim to generate this signal is the wise choice. The CarSim S-Function denotes a CarSim Module, which works as a virtual car. For the interest of steering dynamics, CarSim simulates another vehicle's manual steering process for a given hand-wheel angle with respect to various road surface conditions assumed, while the road reaction torque is available for the user. For the real-time simulation presented in this paper, CarSim is operated for two purposes:

1. Generate the benchmark of the tire position response to the hand-wheel angle from the output of G_1 in Figure 6.2, assuming a straight flat road condition;
2. Generate an estimation of the road reaction torque w_l that is applied to provide low frequency information of w in Figure 6.2(as there is no road roughness assumed).

The block "HW torque" is the system input, which is a pulse signal as shown in Fig 6.4. This input simulates the driver exerting a hand wheel torque with $1Nm$ for five seconds and then releasing it. To verify the performance of the designed EPS system under road disturbance condition, "random number" with different variance cases added into the system to simulate different road conditions.

The input signal is as follows:

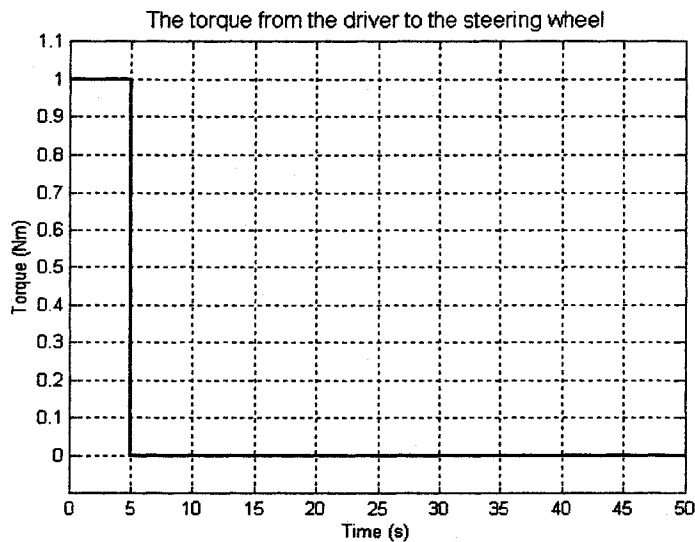


Figure 6.3: System Input Signal

The noise signals are listed below:

- 1) Zero-mean random number noise with variance of 10
- 2) Zero-mean random number noise with variance of 50

A schematic simulink diagram of the test bench is presented as follows in Figure 6.4,

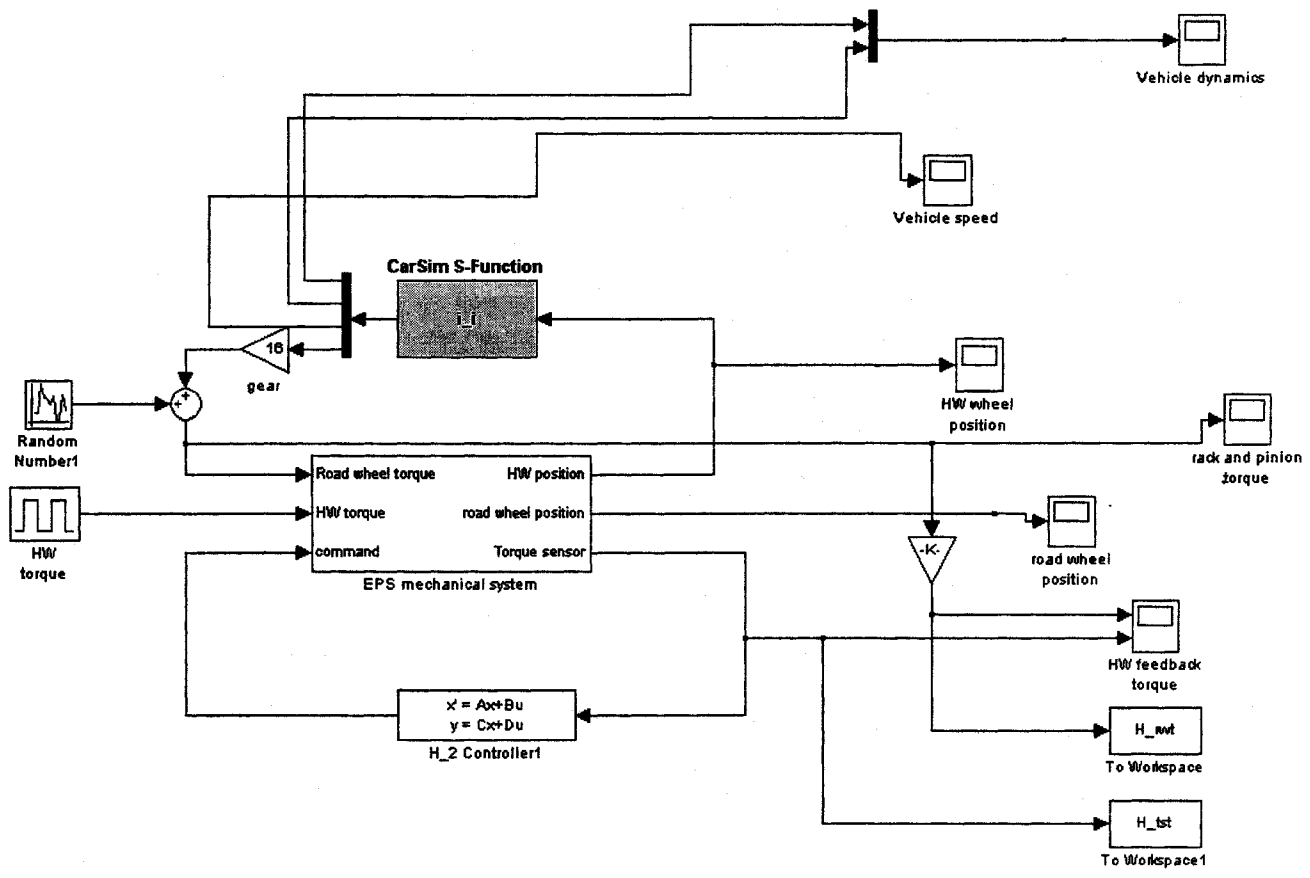


Figure 6.4: EPS System Model with a H_2 Motion Controller

6.3 Off-Line Simulations and Results

H_2 motion controller and P-I motor controller

Basically, what we need to check in the simulations is how well the torque sensor output react to the road reaction torque and the tire wheel angle responds with the human wheel angle, under each of the simulated noise situations. In this off-line simulation of the EPS system with H_2 and $P - I$ controller, noises and other input signals are included and the results are obtained as shown in Figure 6.5 - 6.8.

As can be seen, in each of the cases, the impact of the road roughness surface to the torque sensor output is greatly attenuated by the controller. The H_2 motion well addresses the driving comfortable problem. And the torque sensor output follows driver's steering wheel torque very well, and the whole motion process only takes 7 seconds.

In the figures of the steering wheel angle and rack&pinion angle are for random number with variance 10. (e.g., Figure 6.6) The upper plot stands for the human wheel angle exerted by the driver and the lower one plots the rack&pinion angle generated by the EPS system with the controller. It can be observed that the rack&pinion angle follows the human wheel angle very promptly and accurately, which means, the designed controller enhances the driving performance of the vehicle. And also we attached the benchmark CarSim angle in Figure 6.7. CarSim is assumed to run on the straight flat road surface. It can be judged from the comparison in Figure 6.7 that the proposed EPS controller yield good performance in terms of bringing the steering process on rough road surface close to that on straight flat road surface, while keeping the driver's steering feeling enjoyable-light and less vibration.

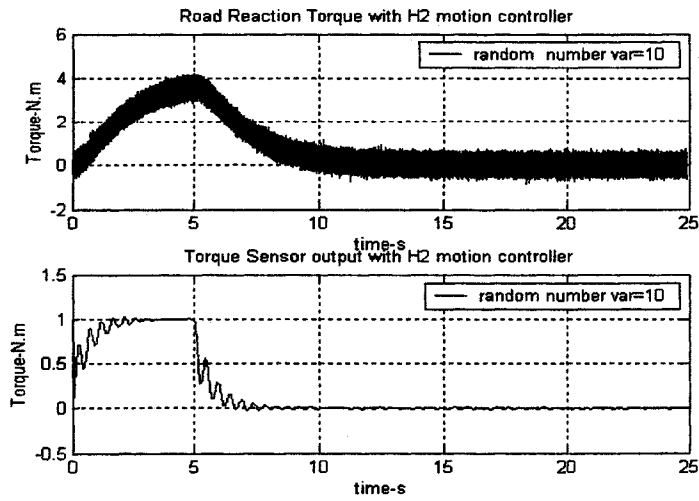


Figure 6.5: Road Reaction Torque and Torque Sensor Output Integrated with H_2 Controller (random number variance = 10)

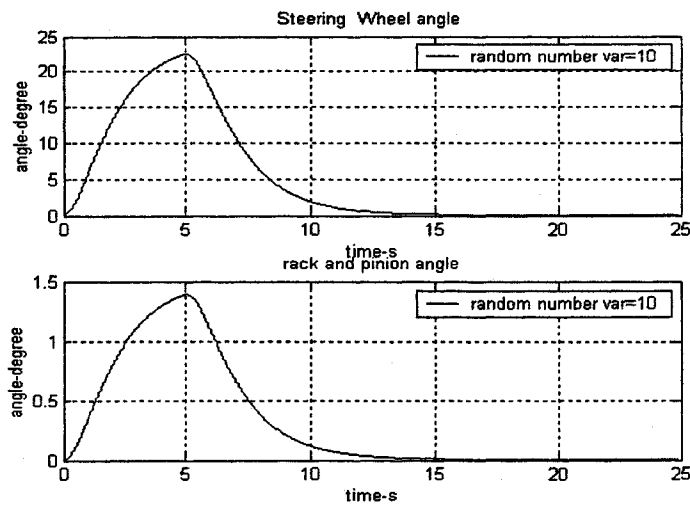


Figure 6.6: Human Wheel Position And Rack & Pinion Angle with H_2 Controller (random number variance = 10)

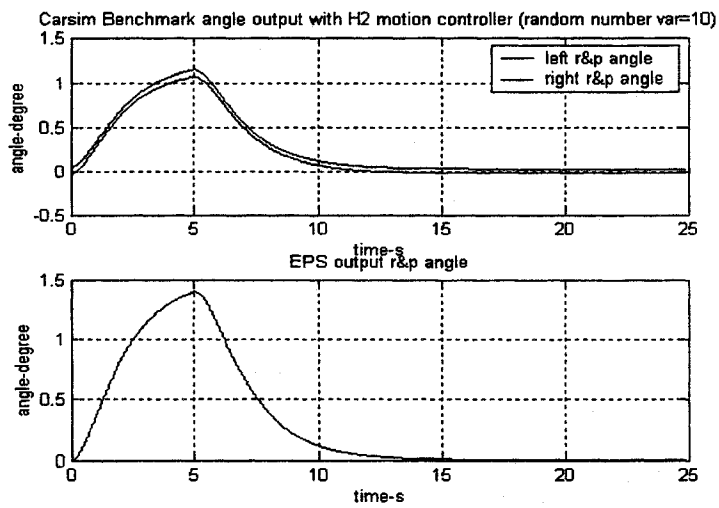


Figure 6.7: CarSim Output Angle Compared with EPS Output Angle with H_2 Controller (random number variance = 10)

In next simulations, the variance of random number is increased from 10 to 50. It is used to simulate the road surface with more roughness. In Figure 6.8, which is the torque sensor output and road reaction torque comparisons, the road roughness is still greatly attenuated by the controller. And the transient response is fast and no overshoot exists.

And also from Figure 6.9, we can find that the rack & pinion angle follows steering wheel angle exactly and also not be affected by the road roughness changing.

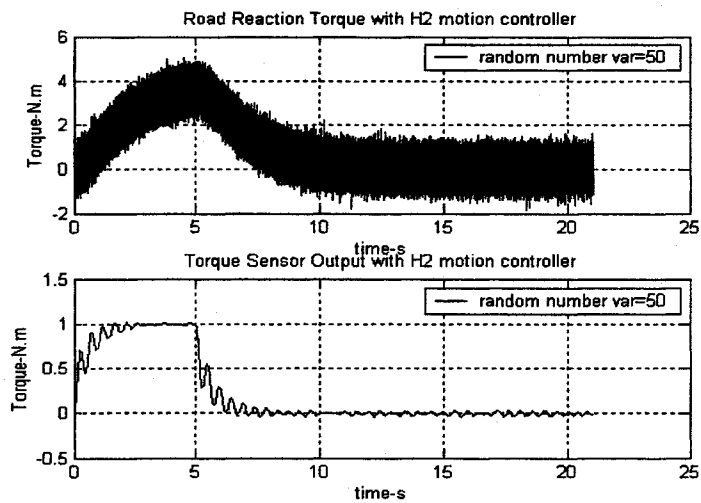


Figure 6.8: Road Reaction Torque And Torque Sensor Output Integrated with H_2 Controller (random number variance = 50)

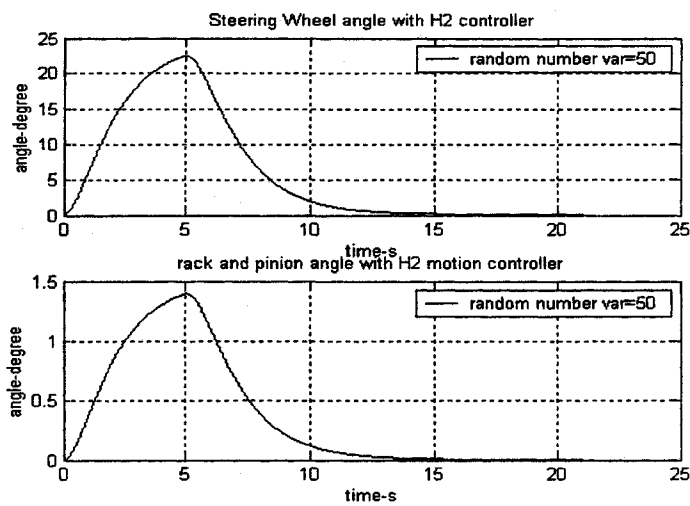


Figure 6.9: Human Wheel Position And Rack & Pinion Angle with H_2 Controller (random number variance = 50)

No Motion Controller

It would be worth of analysis if we compare the performance of the traditional EPS system without the motion controller with that of our proposed EPS systems. Figure 6.10 shows how the torque sensor output responds to the road reaction torque input in an traditional EPS system.

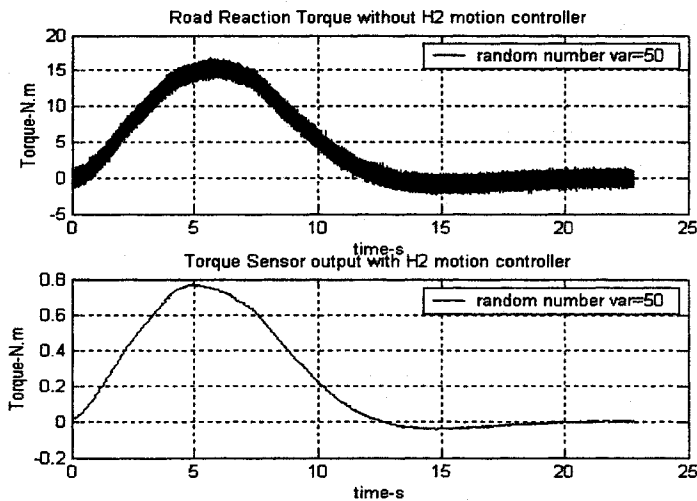


Figure 6.10: Road Reaction Torque And Torque Sensor Output without the Motion Controller (random number variance = 50)

As can be seen from the graph, although the road disturbance can be attenuated in this case, the system without the motion controller will need much more time to reach the stable status. It can be observed that it gradually turn to stable at nearly 25 seconds and at the same around the 13th second, system has slight overshoot. Compared with the system with H_2 motion controller, our motion controller is used to accelerate the system response which only takes 7 seconds for the system to complete the response to the inputs and also follow our input torque signal very well. Therefore, the EPS system with the 2-degree controller (motion controller + motor control) achieves a better performance than those systems with only one traditional controller .

P-I motion controller + P-I motor controller

Again, in this simulation, we need to check how P-I motion controller works in the EPS system. We do not change the P-I torque control, just replace H_2 motion controller with the P-I motion controller

Figure 6.11 shows that P-I motion controller can address the road roughness but achieve worse performance compared with our H_2 motion controller.

In the figures of the steering wheel position and tire position for different P-I motion controller (e.g., Figure 6.12 and 6.13), it can be observed that the tire angle can not turn back to zero, so it shows that P-I motion controller can not work fine in the system.

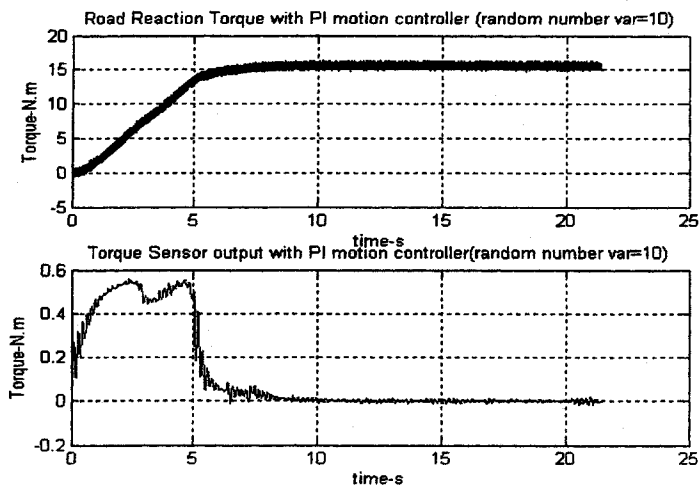


Figure 6.11: Road Reaction Torque And Torque Sensor Output Integrated with $P - I$ Controller, $P=0.05, I=0.3$ (random number variance = 10)

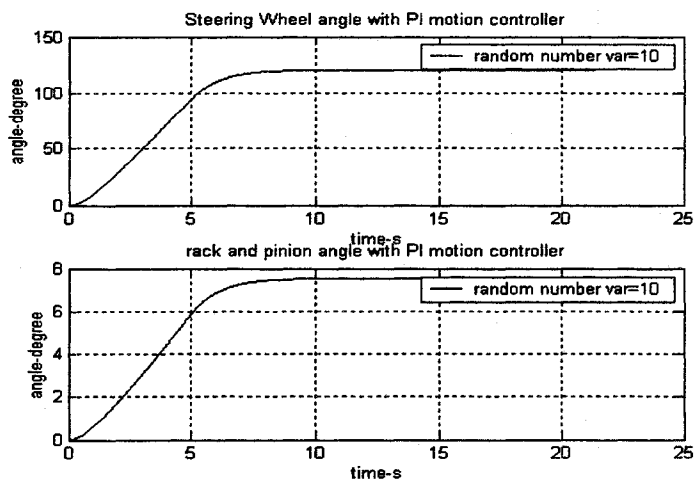


Figure 6.12: Human Wheel Position And Rack & Pinion Angle with $P-I$ Controller, $P=0.05, I=0.3$ (random number variance = 10)

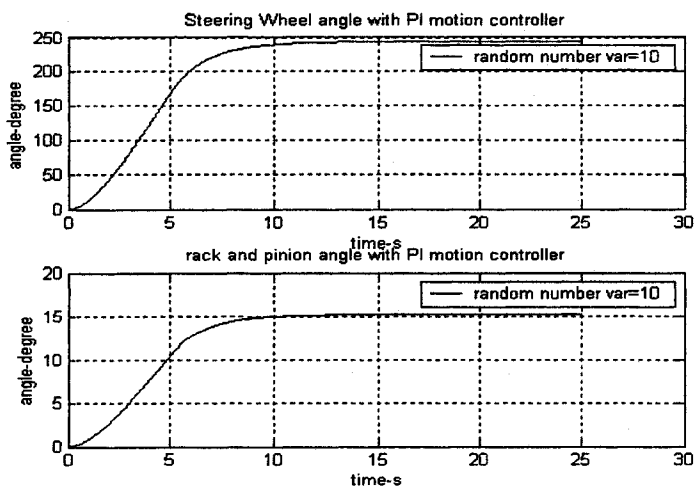


Figure 6.13: Human Wheel position And Rack & Pinion Angle with $P-I$ Controller, $P=10, I=5$ (random number variance = 10)

Simulations for Model Reduction

The simulation results of the 6th order controller are shown in Figure 6.14 and Figure 6.14. Compare with the results obtained from the original 8th order model (Figure 6.8 and Figure 6.9), they are quite similar. The rack & pinion angle follows human wheel angle exactly and the noise is attenuated greatly.

As for the 2nd order controller, the results are shown in Figure 6.17 and Figure 6.18. It can be observed that although the model is reduced substantially, the 2nd order controller still works very well in the system.

From these figures, it can be seen that the controller after model reduction won't affect the overall performance. It proves that the reduced order motion controller will be good a candidate to implement into the practical system.

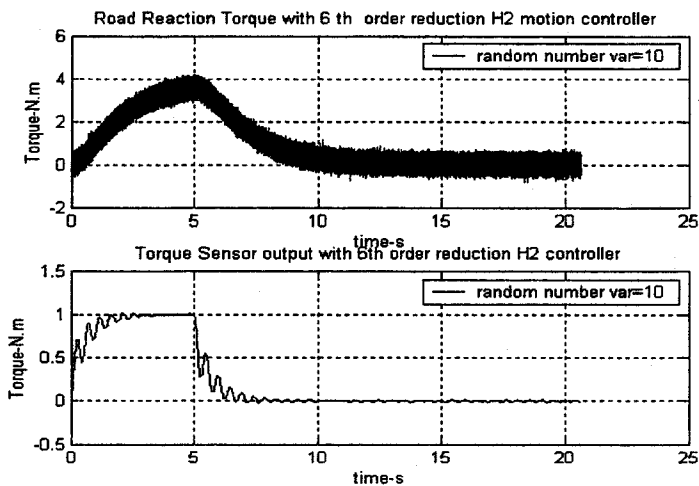


Figure 6.14: Road Reaction Torque And Torque Sensor Output Integrated with H_2 Controller (6th order controller model, random number var = 10)

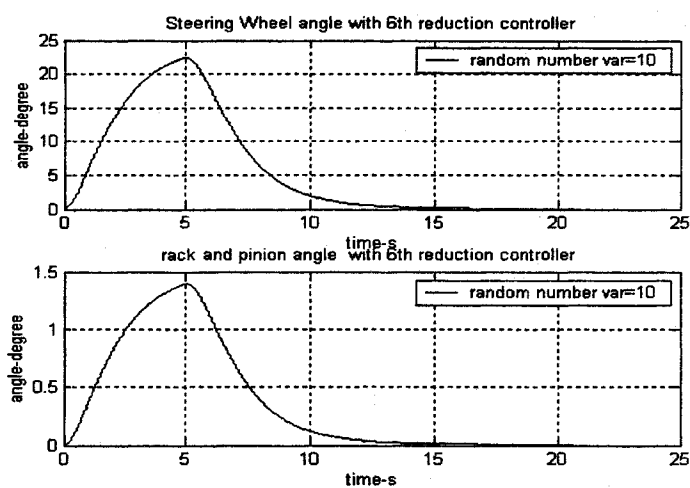


Figure 6.15: Human Wheel Position And Rack & Pinion Angle with H_2 Controller (6th order controller model random number var = 10)

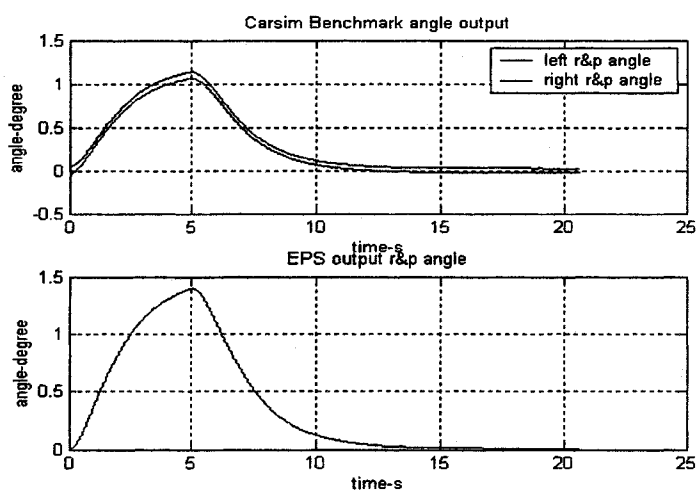


Figure 6.16: CarSim Output Angle Compared with EPS Output Angle with H_2 Controller (6th order controller model random number var=10)

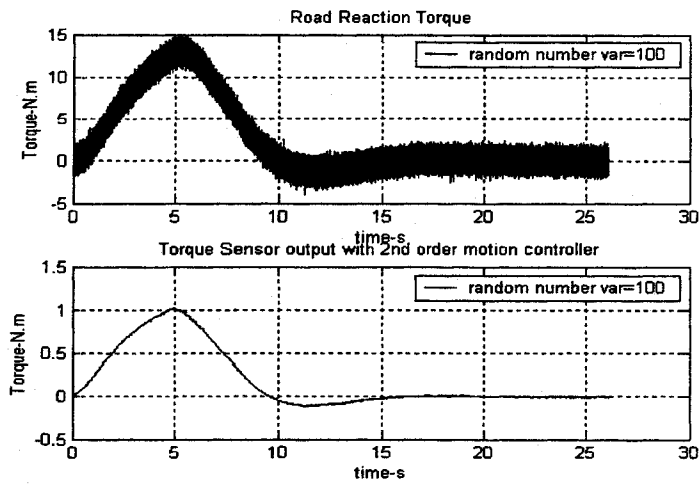


Figure 6.17: Road Reaction Torque And Torque Sensor Output Integrated with H_2 Controller (2th order controller model random number var = 100)

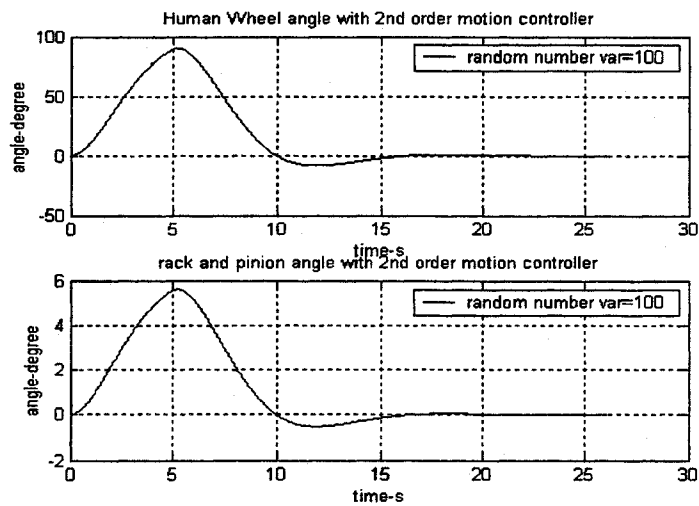


Figure 6.18: Human Wheel position And Rack & Pinion Angle with H_2 Controller (2nd order controller model random number var=100)

6.4 Real-Time Simulations

In a competitive world, using real-time simulation rather than numerical simulation (off-line simulation) provides a significant advantage. Real-Time simulation can minimize risks, improve reliability, and bring a system into operation more quickly, while numerical simulation results may not be reliable, sometimes only qualitative. Therefore, Opal-RT and CarSim-RT platforms are used to provide the real time simulations for the EPS model developed in this research. RT-LAB software runs on a hardware configuration consisting of Command Station, Compilation node, Target nodes, Communication links (real-time and Ethernet), and the I/O boards. It is configured on Windows platform for the Command Station. Simulations can be run entirely on the Command Station computer, but they are typically run on one or more target nodes. For real-time simulation, the preferred operating system for the target nodes is QNX. When there are multiple QNX nodes, one of them is designated as the compilation node. The Command Station and target node(s) communicate with each other using communication links, and for hardware-in-the-loop simulations target nodes may also communicate with other devices through I/O boards.

Command Station

The command Station is a PC workstation that operates under Windows operating system, and serves as the user interface. The Command Station allows users to:

- 1) Edit and modify models
- 2) See model data
- 3) Run the original model under its simulation software (simulink)
- 4) Generate code
- 5) Separate code

- 6) Control the simulator's GO/STOP sequences

Target Nodes

The target nodes are real-time processing and communication computers that use commercial processors interconnected by an Ethernet adapter. These computers can also include a real-time communication interface like FireWire or cLAN (depending on the selected OS), as well as I/O boards for accessing external equipments. The real-time target nodes perform:

- 1) Real-time execution of the model's simulation
- 2) Real-time communication between the nodes and I/Os
- 3) Initialization of the I/O systems
- 4) Acquisition of the model's internal variables and external outputs through I/O modules
- 5) Implementation of user-performed online parameters modifications
- 6) Recording data on local hard drive, if desired
- 7) Supervision of execution of the model's simulation, and communication with other nodes.

Compilation Node

The compilation node is used to:

- 1) Compile C code
- 2) Load the code onto each target node
- 3) Run the original model under its simulation software (simulink)

- 4) Debug the user's source code (S-function, user code block, etc.)

Communication

Firewire real-time link: The real-time communication link works using FireWire (IEEE P-1394) or cLAN interfaces. Both ensure:

- 1) Real-time communication between slaves, and between the target nodes and the I/O
- 2) Synchronization between the I/O boards and target nodes.

Ethernet Link: An Ethernet link is used to transfer simulation models and run-time data between the Command station and the target nodes.

I/O boards: Both analog and digital I/O boards are supported by RT-LAB. These allow connection to external equipment for applications such as Hardware-In-Loop.

Real-Time Simulations for EPS systems

For the real-time EPS system realization, two nodes are needed to implement the simulation. Therefore it is necessary to build a distributed model for RT-LAB. There are three parts in the whole model. One is called the master module, beginning with SM. Another module is called slave module, beginning with SS. The command station used to input signal and accept the output signal is called the console module, beginning with SC.

The model's real-time calculation is implemented in the master subsystem, which is used to link to CARSIM-RT to simulate the tire model.

The slave subsystems are still used to perform calculations in the model, and also do the real communication with master subsystem. For real-time applications, there can be

more than one slave. The number of slaves depends on the simulated model complexity and the number of target nodes availability. In EPS system, EPS mechanical simulink model is grouped into the slave system which can communicate with the tire model through a designed real-time link with TCP/IP protocol.

The console subsystem contains all the simulink blocks related to acquiring and viewing data (scope, manual switch, To workspace-type blocks, etc.). When creating a subsystem, Opalcomm blocks must be inserted into the console subsystem to acquire data from the model. Any simulink model that will run in RT-LAB platform should have only one Console block.

For our simulation, the schematic diagram of computer work is in the Figure 6.19 as follows:

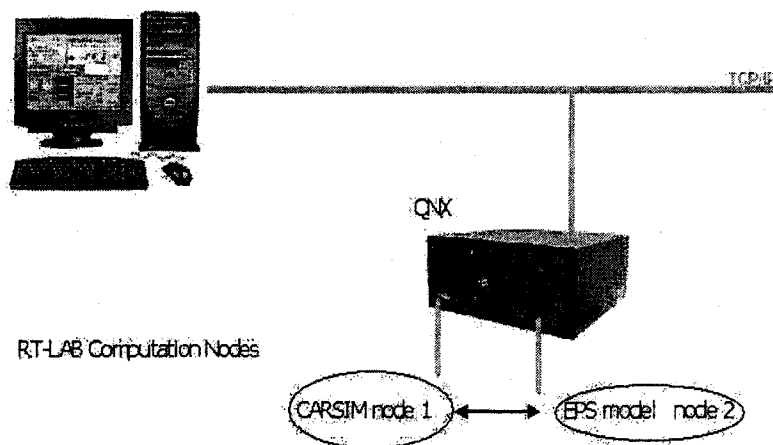


Figure 6.19: Schematic Diagram of Computer Work

Problems and Solutions for the Real-time Simulation

Step size determines the time interval between subsystem's consecutive calculation steps. If, for only one single node, the minimum step size is $15\mu s$; for 2 nodes, the minimum step size is equal to $100\mu s$. The EPS real-time model has two nodes, so the minimum step size is $100\mu s$.

It is known in the former chapter that the motor with P-I controller system close loop

transfer function diagram is shown below in Figure 6.20:

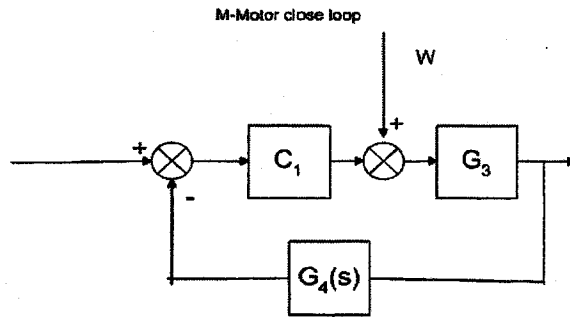


Figure 6.20: Motor with Controller System block

We find that the motor close loop function with disturbance has higher frequency poles which exceeds the 0.001 sampling frequency offered by the QNX system. Using an approximated model is the better way to fix this problem.

From the diagram we find that output Y is added by two inputs (EMF input W and reference R) So we get the the equation 6.5:

$$Y = R \frac{C_1 G_3}{1 + C_1 G_3 G_4} + W \frac{G_3}{1 + C_1 G_3 G_4} \quad (6.5)$$

We can do the approximated transfer functions for reference signal R and EMF signal W separately. The transfer function for reference signal is equation 6.6

$$G_M = \frac{(3223S^2 + 28670S + 980) \times 12}{0.000237S^3 + 80.64S^2 + 727.3S + 24.5} \quad (6.6)$$

The poles of this transfer function are $p_1 = -3.4025 \times 10^5$, $p_2 = -8.9852$, $p_3 = 0.033814$, respectively; For p_1 , the pole is very faster than the fix-step size of 0.001. Therefore it can be accepted by the real-time system.

In order to run the real time simulations for the model, we need to transform the transfer function of the whole model, with the steps shown as follows:

- 1) Factorize $G_r = \frac{(3223S^2 + 28670S + 980) \times 12}{0.000237S^3 + 80.64S^2 + 727.3S + 24.5}$. After factorization, we can get three transfer functions:

$$sys1 = \frac{0.0197}{s+0.03381}, \quad sys2 = \frac{-4.967}{s+8.985}, \quad sys3 = \frac{1.36 \times 10^7}{s+3.402 \times 10^5}$$

- 2) From the transfer function 3, we know the pole of this transfer function is of a very high frequency therefore it can be sampled by the fix step size as 0.001 s. Because this pole, compared with the other two poles, is far away from the imaginary axle, for an approximation of the model this pole can be omitted. Before removing the pole, we need to extract its DC gain:

$$gain = \lim_{s \rightarrow 0} \frac{1.36 \cdot 10^7}{s + 3.402 \cdot 10^5} = 39.97.$$

Therefore the approximated system transfer function becomes:

$$sysapp = sys3 + sys3 + gain = \frac{1.36 \cdot 10^7 S^2 + 1.21 \cdot 10^8 S + 4.135 \cdot 10^6}{3.402 \cdot 10^5 S^2 + 3.069 \cdot 10^6 S + 1.034 \cdot 10^5}.$$

Same way we approximate the transfer function for EMF input signal W input

- 1) Factorize $G_w = \frac{0.158S^2 + 1.4S}{0.000237S^3 + 80.64S^2 + 727.3S + 24.5}$.
- 2) $syswapp = gainw + sysw1 + sysw2 = \frac{666.7S^2 + 5907S + 2.84 \cdot 10^{-14}}{3.402 \cdot 10^5 S^2 + 3.069 \cdot 10^6 S + 1.034 \cdot 10^5}$.

The approximated model for real-time simulation is shown in Figure 6.21:

Real-Time Simulation Results

Since most of the simulation results have already been obtained in the off-line simulations, we just need to list some of the real time simulation results here to verify with the off-line simulations. In addition, because the model used to run the real-time simulations is already an approximated model, the real-time robustness test is also performed at the same time.

Figure 6.22 - 6.24 show the real-time simulation results of the system. We also give the CarSim angle output comparison with EPS output angle. We can see that the results are very close to those off-line results. Furthermore, its real time model passes the robustness test.

The RT-LAB real-time simulations verify that the new 2-degree controller is effective not only theoretically but also practically.

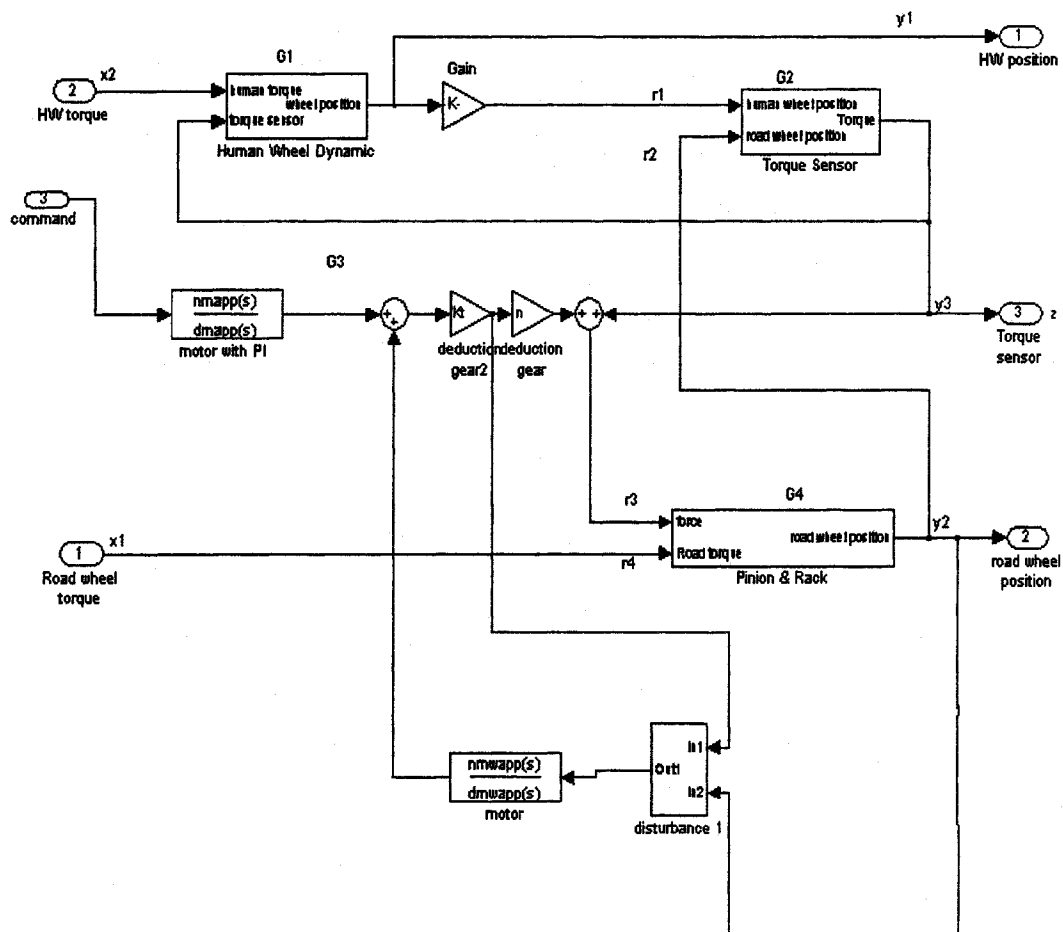


Figure 6.21: EPS System Approximated Simulink Model for Real Time Simulation

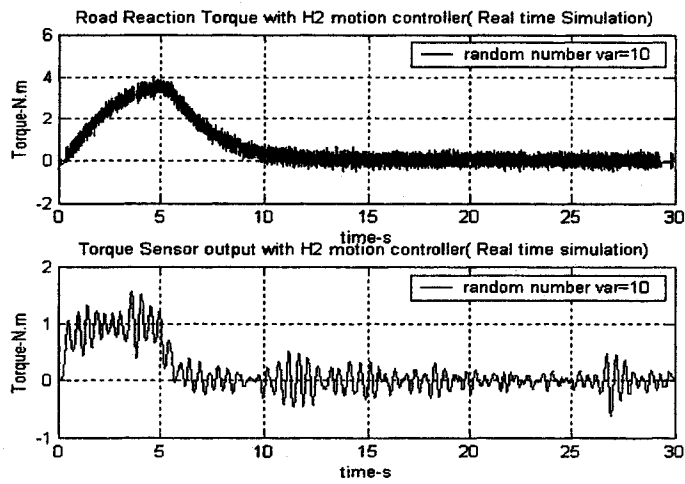


Figure 6.22: Road Reaction Torque and Torque Sensor Output Integrated with H_2 Controller (Real-Time Simulation, random number variance = 10)

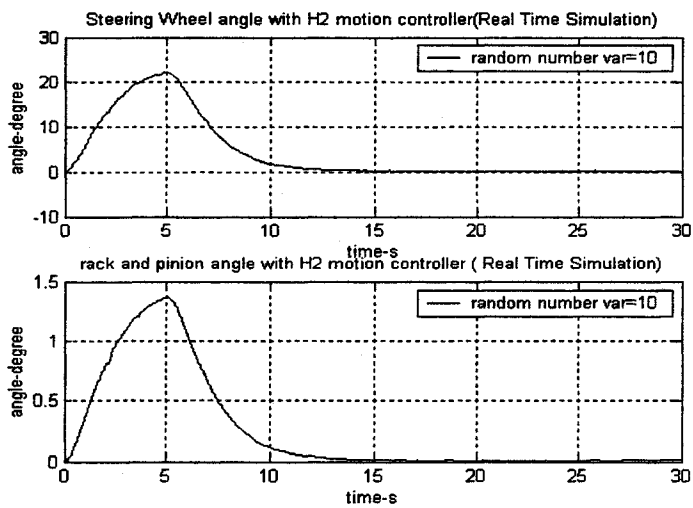


Figure 6.23: Human Wheel position and rack and pinion angle with H_2 Controller (Real-Time Simulation, random number variance = 10)

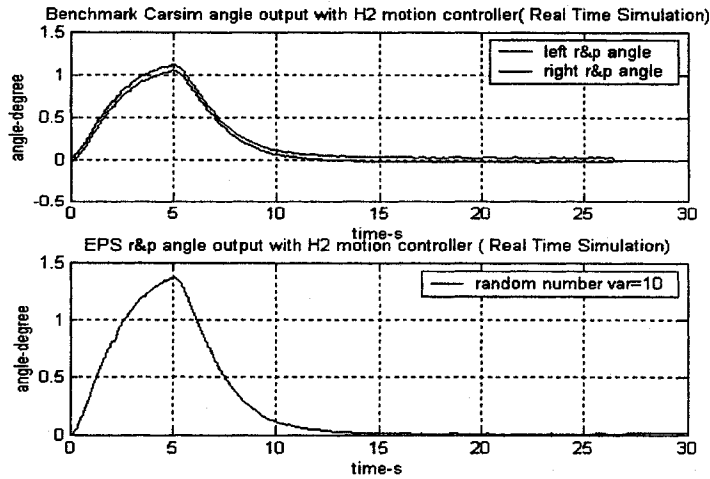


Figure 6.24: Carsim Output Angle And EPS Output Rack& Pinion Angle with H_2 Controller (Real-Time Simulation, random number variance = 10)

Figure 6.25 shows the real-time simulation results of the system with reduced model . From the Figure 6.25, we can find the system equipped with the reduced order controller not only the offline simulation but also real time simulation is very close to the original 8th order model . So the reduced order controller will be a good candidate for the real implement to the real system or in hardware-in-the-loop tests.

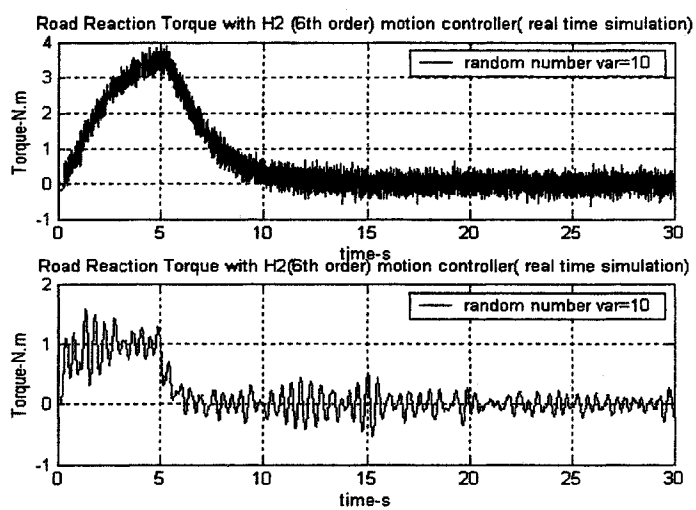


Figure 6.25: CarSim Output Angle And EPS Output Rack& Pinion Angle with H_2 Controller (Real-Time Simulation, random number variance = 10)

Chapter 7

Conclusion and Future Work

7.1 Conclusion

Power steering, once an option, is becoming standard equipment on some vehicles and more are expected to be implemented. Power steering has evolved over the years from a simple control valve and external hydraulic ram on the regular steering mechanism to integrated rack and pinion systems with variable assist under different driving conditions. Now electric power steering is making inroads into the marketplace and it offers several advantages.

There is a lot of design work and technology in the electric steering systems themselves, but the use of electric systems simplifies vehicle assembly and frees up space in the engine compartment which make manufacturers work simpler than before. Hydraulic steering requires a pump mounted on the engine, a belt to drive the pump, hoses to connect the pump to the steering gear and fluid to transfer the energy from the pump to the steering gear. All these mechanical components can now be taken the place of cheaper and simpler electric components. This may not sound like much, but in design terms, it is significant.

For drivers, the big benefit of electric power steering has to be fuel economy. Engineers think of up to five percent gain in fuel economy because the systems only use power when the wheels are turned compared to hydraulic systems that pump fluid all the time the engine is running.

Till now, a lot of EPS model and control algorithms are developed to keep up with the growing demands for the driver. In this thesis, we give a developed EPS model and

propose a two controller design strategy for the whole system. Based on the EPS model and optimal control algorithm, we here present a H_2 controller, the optimal control results and comfortable driver steering feeling can be offered. From the simulation results, system overall performance is greatly improved through the controller.

7.2 Future work

7.2.1 Hardware-in-the-loop

Because the off-line simulation is validated by the real-time simulation in this thesis, further tests around controller implementation is necessarily. A DSP board with a real time virtual vehicle module can be used to implement hardware-in-the-loop. It is good direction for saving cost to set up the whole real system .

7.2.2 Fault Tolerant Implementation

In order to gain more powerful control purpose, fault tolerant can be incorporated into the controller. With the fault tolerant performance, even the failure or measurement mistake of the current sensor, the EPS system still can work properly. So this still can be a research object for the EPS system.

Appendix A

Coefficients used EPS system

Steering wheel dynamics:

Inertia moment: $J_{hw} = 0.033$

Damping ratio: $B_{hw} = 0.02$

Torque Sensor:

Damping ratio: $B_s = 0.05$

Stiffness coefficient: $K_s = 80$

Motor:

Inertia moment: $J_m = 0.00395$

Damping ratio: $B = 0.035$

Resistance: $R = 0.37$

Inductance: $L = 0.0015$

Electromotive force constant: $K_t = 0.5$

KE: 53V/1000rpm

Rack and Pinion:

Inertia moment: $J_r = 0.0308$

Damping ratio: $B_r = 0.5$

Appendix B

CARSIM-RT and OPAL-RT Set up

CarSim RT for RT-LAB test bench setup procedure:

Open CarSim software:

First, open the CarSim software and click on ' Model Type '. Select ' Transfer to RT-LAB Target ' from the list of options. A check mark will appear beside the selection and the button name will now change to 'Model Type: RT-LAB Target'. (If you are running from an offline simulink model, select ' Type: Simulink ' instead).

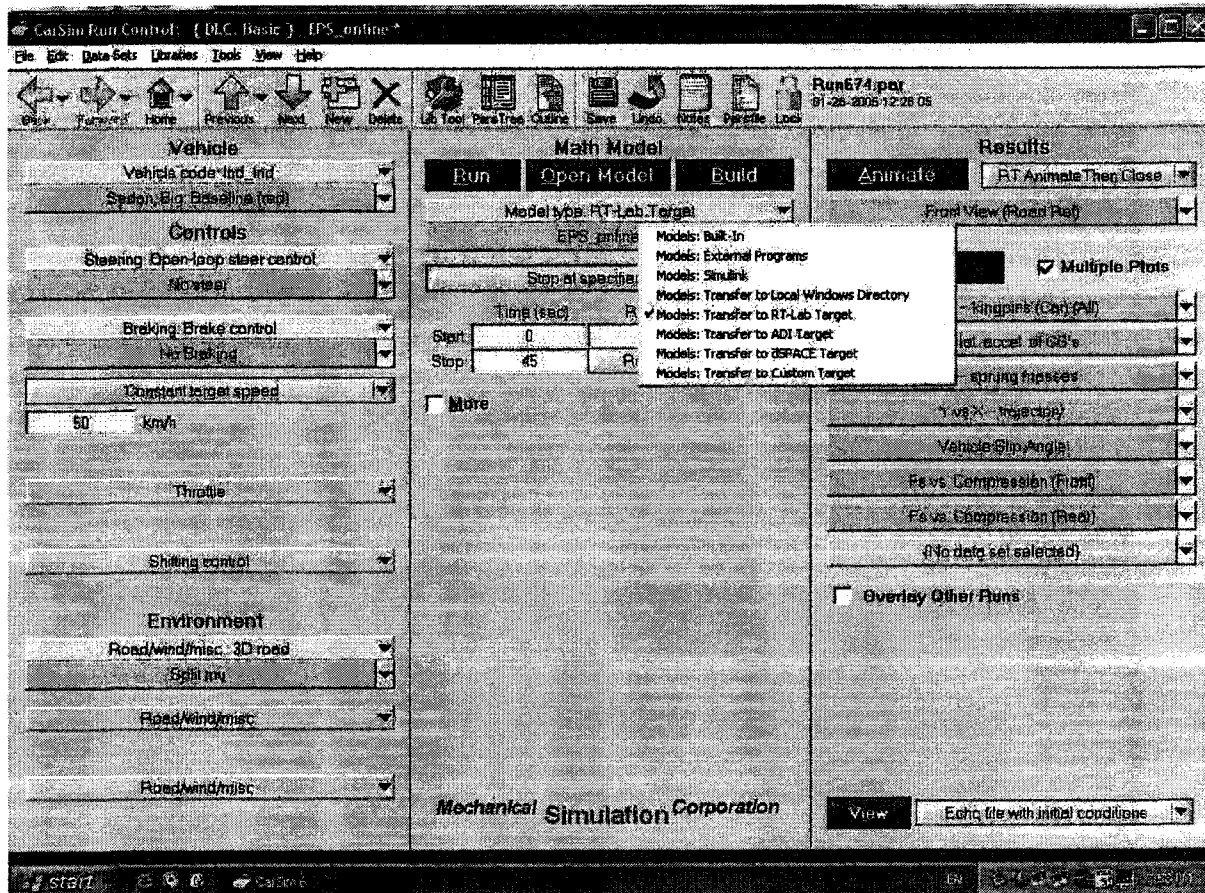


Figure .1: Open CARSIM-RT

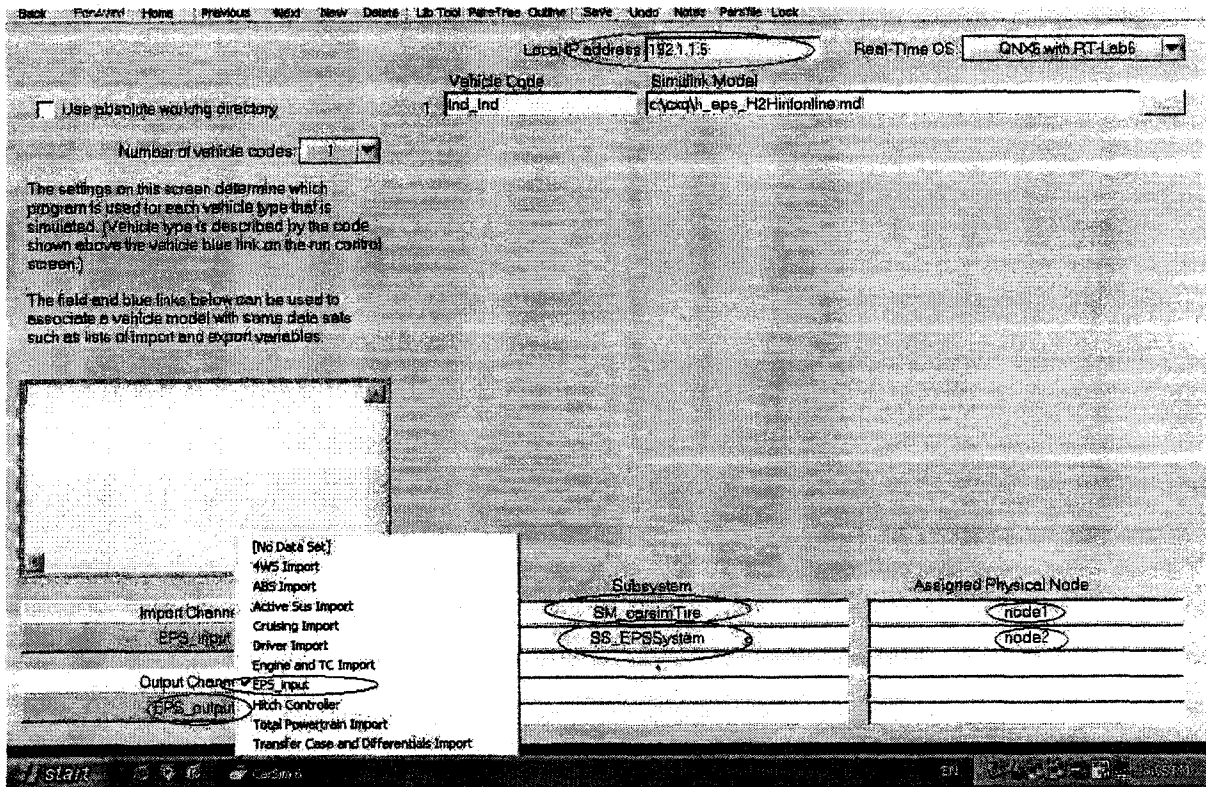


Figure .2: CARSim-RT node configuration

Next, double-click on 'EPS-Online' which is directly below the 'Model Type-RT LAB' button. A pop-up window will then appear as shown in Figure B.2. The 'Local IP Address:' value is set to 192.1.1.5 which is the IP address of the command station that needs to be filled out.

In the bottom left corner of the window, we can find two options named 'Import Channel' and 'Output Channel'. These options need to be defined and here we set the import and output channels as 'EPS input' and 'EPS output' respectively from the list of selections.

For the 'Subsystems' and 'Assigned Physical Nodes' fields, the corresponding names and designated nodes entered must match the SM and SS modules in the RT simulink model. Their node designations 'node1' and 'node2' must also be configured in OPAL-RT which will be explained later.

After setting up the CARSIM configurations, open the OPAL-RT program as shown below in Figure .3. In the ' Model Selection ' area, click on ' Open Model ' to select the model required for the simulation.

Here we shall pay more attention to choose the ' Target platform ' as ' Neutrino ' as shown in Figure .3.

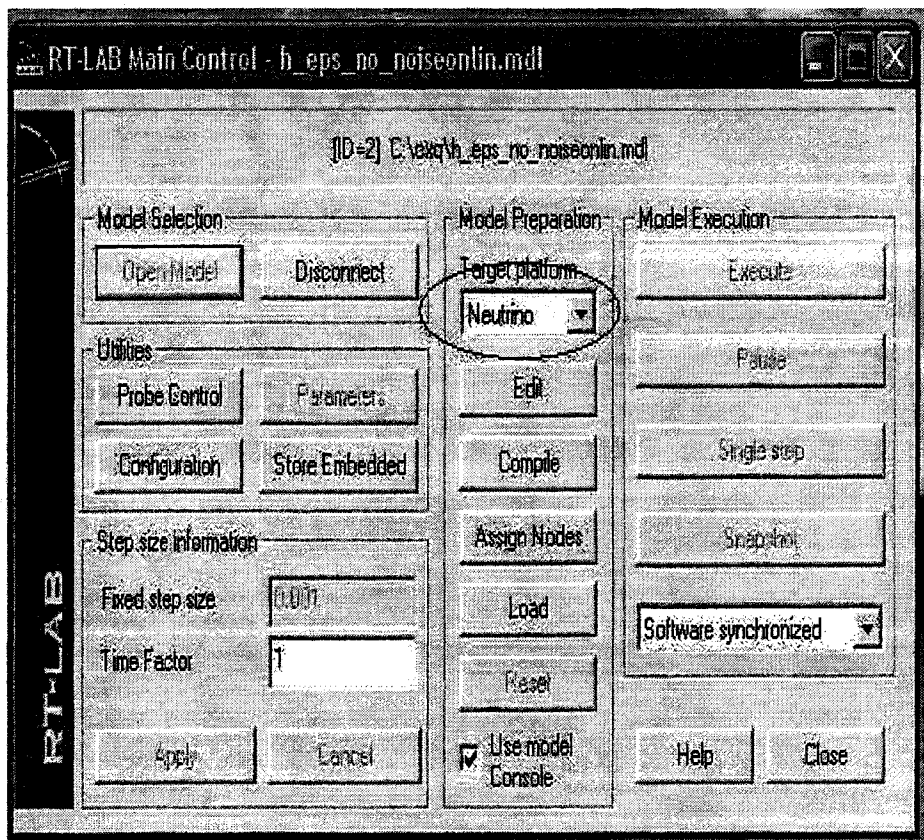


Figure .3: OPAL-RT main configuration Window

In the 'Utilities' area, double-click on ' Configuration ' for more advanced settings of OPAL-RT. Then a window pop out as show in Figure .4

In ' Before Opening Model ', we can add data files to OPAL-RT and here we set it to ' H2datanew'(eg.). ' Runall.par and simfile ' are necessarily for running CarSim-RT and are automatically added.

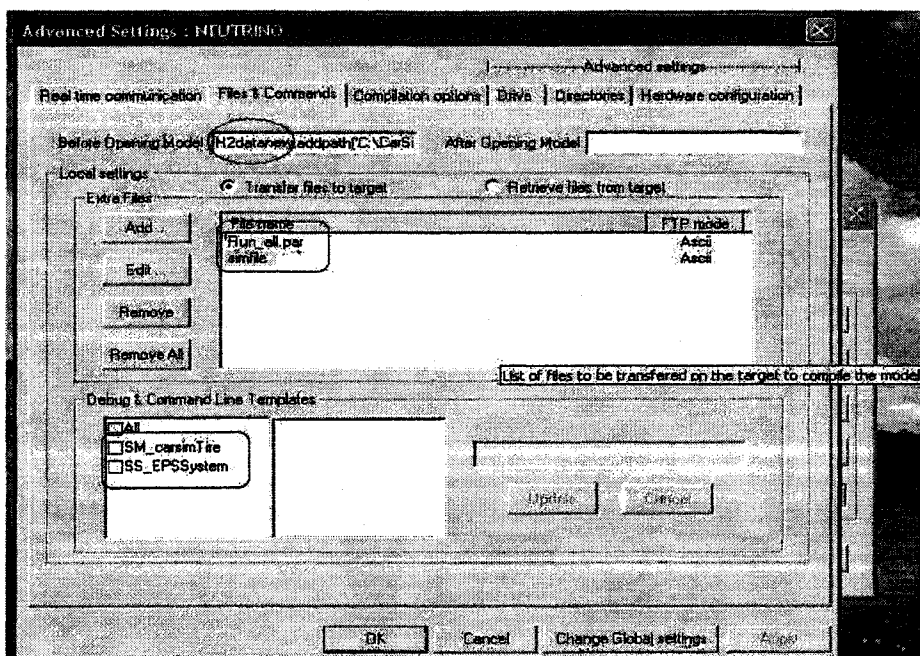


Figure .4: Advanced Settings1

Next, we need to configure the two nodes mentioned earlier in Figure .2. To do so, select the ' Hardware configuration ' tab and the nodes can be configured with different IP addresses here. Their names must match those mentioned in Figure .2 and here they are defined as ' node1 ' and ' node2 '.

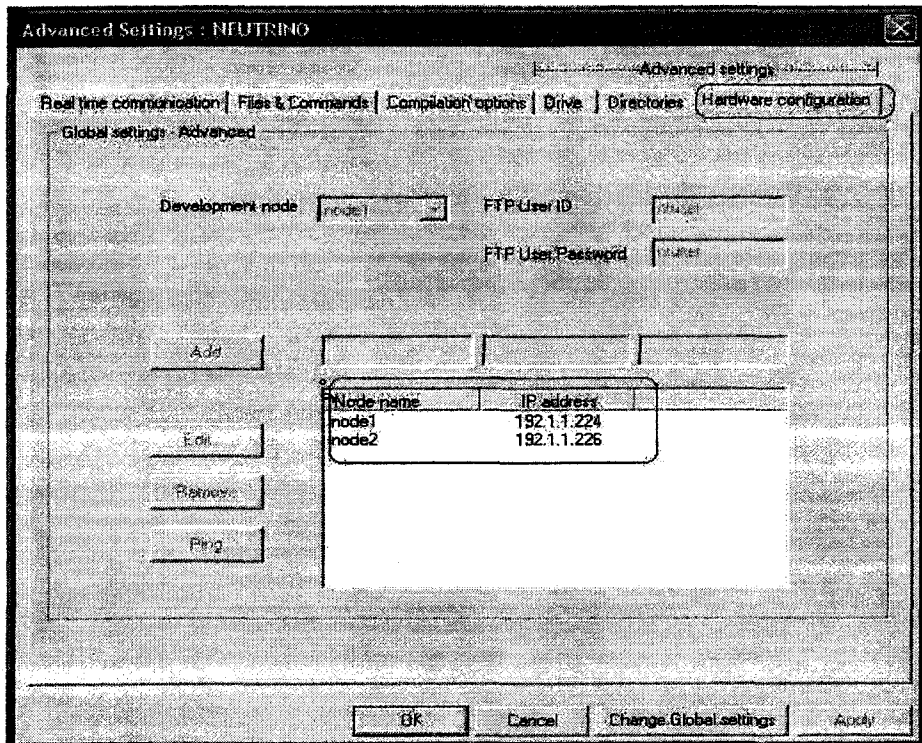


Figure .5: Advanced Settings2

We can click the ' Hardware configuration ' page, we can find two nodes with different ip address are configured there as shown in Figure .5. Their names shall be the same as the name in Figure .2. Here the node names are named as node1 and node2. The real time model for EPS simulation is shown in Figure .6

Before we can start the real-time simulation, we need to modify the parameters so that the CarSim licence file can be automatically loaded into OPAL-RT. To do so, open the RT simulink file first and then click on 'SS' to find the state space model. Change all the A, B, C, D matrix values to equal one first.

After we've finished the configurations of all former procedures, we must first run the

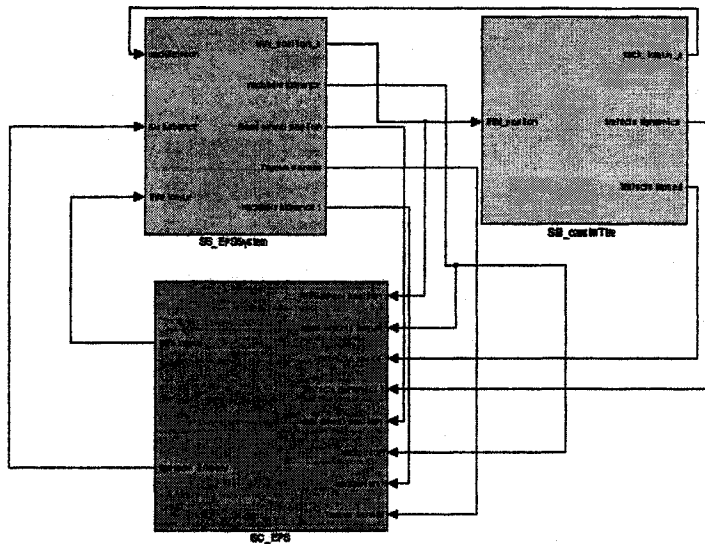


Figure .6: EPS System Real-Time Model

model through CarSim main window as shown in Figure .1. Without this step, OPAL-RT can not communicate with CarSim. After completing this required step, we can then run the actual model in OPAL-RT.

Now return to the window show as in Figure .3, there are three buttons in the 'Model Preparation' area as shown in Figure .3. Click on ' Compile ', ' Assign Nodes ' and ' Load ' respectively in order to set-up the model's real-time simulation. If there is any compile error, click on ' Edit Model ' to check and correct the error. Only after all the errors have been eliminated, we can then continue. Finally, when these three steps are successfully completed, click on ' Execute ' to run the CARSIM-RT real-time simulations.

Bibliography

- [1] F. J. Adams, "Power Steering Road Feel", SAE Paper 830998, 1983.
- [2] Aly Badawy, Jeff Zuraski, Farhad Bolourchi and Ashok Chandy, "Modeling and Analysis of an Electric Power Steering System", SAE TECHNICAL PAPER SERIES, 1999-01-0399
- [3] J. Baxter, "Analysis of Stiffness and Feel for a Power-Assisted Rack and Pinion Steering Gear", SAE Paper, 880706, 1988.
- [4] "CarSim User Manual Version 5.11", Mechanical Simulation Corporation, 709 West Huron, Ann Arbor, MI 48103.
- [5] R. Y. Chiang, M. G. Safonov, "Robust Control ToolBox, for use with MATLAB", the MATHWORKS Inc.
- [6] Rodriguez, F.; Uy, E.; Emadi, A.; "Brushless DC motor drive for steer-by-wire and electric power steering applications " ,Electrical Insulation Conference and Electrical Manufacturing & Coil Winding Technology Conference, 2003. Proceedings , 23-25 Sept. 2003 ,Pages:535 - 541
- [7] G. R. Ferries, and R. L. Arbanas, "Control/Structure Interaction In Hydraulic Power Steering Systems", *Proc. of the ACC*, Vol.2, pp. 1146 - 1151, 1997.
- [8] Manu Parmar and John Y. Hung, "Modeling and Sensorless Optimal Controller Design for an Electric Power Assist Steering System", *Proc. of the IECON 02*), Vol.3, pp. 1784-1789, 2002.

- [9] Thomas Gillespie , "Fundamentals of Vehicle Dynamics" ,Society of Automotive Engineers, Inc, 1992
- [10] N. Mohan, T. M. Uneland and W. P. Robbins, "Power Electronics-Converters, Applications, and Design" , 3rd Ed., John Wiley & Sons, 2003.
- [11] N. Sugitani, Y. Fujiwara, K. Uchida, and M. Fujita, "Electric Power Steering with H-infinity Control Designed to Obtain Road Information", proc. of the ACC,Vol.5, pp. 2935-2939, 1997.
- [12] Jeha Ryu, HeeSoo Kim, "Virtual environment for developing electronic power steering and steer-by-wire systems", Intelligent Robots and Systems, 1999. IROS '99. Proceedings. 1999 IEEE/RSJ International Conference on , Vol.3 , pp.1374 - 1379 ,1999 .
- [13] Opal-Rt, "RT-LAB 6.0 user's manual"
- [14] Y.Gene Liao , H.Isaac Du , "Modeling and analysis of electric power steering system and its effect on vehicle dynamic behavior" , Int . J. of Behicle Autonomous Systems (IJVAS) , Vol. 1, No. 2 , 2003
- [15] Anthony, W. Burton, "Innovation Drivers for Electric Power-Assisted Steering", Control Systems Magazine, IEEE , Vol. 23 ,pp.30 - 39 Issue: 6 , Dec. 2003.
- [16] A. T. Zarembo, M. K. Liubakka, R. M. Stuntz, "Control and Steering Feel Issues in the Design of an Electric Power Steering System", Proc, of the Acc, pp. 36-40, 1998.
- [17] K. Zhou, J. C. Doyle and K. Glover, "Robust and Optimal Control", Prentice Hall, upper Saddle River, NJ 07458.
- [18] K. Zhou, J. C. Doyle and K. Glover, "Essentials of Robust Control", Prentice Hall, upper Saddle River, NJ 07458.

VITA AUCTORIS

NAME: XiaoQun Chen

PLACE OF BIRTH: Shanghai, China

YEAR OF BIRTH: 1977

POST-SECONDARY EDUCATION
AND DEGREES: WeiYu High School
Shanghai, China
1992-1995, B.Sc

University of Electronic Science and Technology of China
Chengdu, Si Chuan, China
1995-1999, B.Sc

University of Windsor
Windsor, On, Canada
2004-2005, M.Sc

RELATED WORK EXPERIENCE: Software Engineer
Shanghai Bell- Alcatel Corporation
1999.7-2003.4